A Glider-Mounted Shadowgraph Camera as a Tool for Quantifying Meso- And Gelatinous Zooplankton Distribution

by

Natasha J. Hynes
B.Sc. Marine Biology, Dalhousie University, 2018

A Thesis Submitted in Partial Fulfillment of
the Requirements for the Degree of

Master of Science

In the Graduate Academic Unit of Biological Sciences

Supervisor: Kimberley Davies, PhD, Biological Sciences

Examining Board: Chris Gray, PhD, Biological Sciences, Chair

Rémy Rochette, PhD, Biological Sciences

Christian Reiss, PhD, Southwest Fisheries Science Center, Antarctic Ecosystem Research Division, National Oceanic and Atmospheric Administration

Anaïs Lacoursière, PhD, St. Andrews Biological Station, Fisheries and Oceans Canada

This thesis is accepted by the
Dean of Graduate Studies

THE UNIVERSITY OF NEW BRUNSWICK

April, 2024

ABSTRACT

Monitoring zooplankton populations, especially those of energy-rich copepods, is of interest due to their roles as prey for many commercially important and endangered marine species. Autonomous sampling could help improve fine-scale temporal and spatial monitoring, complimenting conventional methods. Here, I evaluate the performance of a prototype, glider-mounted shadowgraph camera for estimating zooplankton identifications and concentrations. The evaluation was completed via a gear-comparison with standard samplers (a MultiNet Midi and UVP6-HF). Copepods were the most abundant taxon in the zooplankton community and the shadowgraph yielded mostly definite identifications, while the UVP6 had more uncertainties. The shadowgraph and UVP underestimated concentrations compared to the MultiNet, yet correlations were significant with both imaging sensors. The shadowgraph, with a Spearman correlation of 0.73 with the MultiNet, excelled at detecting vertical copepod layers and further studies should explore the shadowgraph's ability to detect diel-vertical migration and develop machine learning tools to aid finer taxonomic identification.

DEDICATION

For Scott and Jerry

ACKNOWLEDGEMENTS

I would first like to thank my supervisor Kim Davies for her confidence in me and her support and mentorship throughout the course of this degree. Another thank you to those in the Davies Lab including Delphine Mossman, Cody Carlyle, Andréa Mesquita, Kate Indeck, and Jill Carter for your friendship and R expertise, Emma Chaumont for being my first mentee and helping to process plankton imagery, and to Gina Lonati for putting more seats at the table. I would also like to thank Moira Brown and Claire Goodwin for being such great mentors throughout my career thus far. It has been incredible being surrounded by such intelligent and kind people.

This thesis has benefitted greatly from my committee members Christian Reiss and Rémy Rochette because of their generosity both in resources and expertise. Many thanks also to Randy Cutter at NOAA for your technical support while processing the shadowgraph imagery. I have much gratitude for the CEOTR crew, especially Jude van der Meer (along with Adam Comeau, Alex Cerra, and Zach Viva), who helped prep both the glider and myself to make the deployments for this project go as smooth as possible. Williamson and Associates were also an immense help with pre-deployment shadowgraph testing. Another huge thank you to the folks who made fieldwork possible including Captain Danny Barker and Jeremy Barker, the Canadian Whale Institute, and those who crewed the cruise days for my project.

Thank you to my friends and family who have no idea what I do but listen attentively anyway. And finally, thank you to Scott Saunders and my little Jerry – for being the best part of everything.

TABLE OF CONTENTS

LIST OF TABLES

LIST OF FIGURES

LIST OF SYMBOLS, NOMENCLATURE, ABBREVIATIONS

UVP – Underwater Vision Profiler

UVP5 – Underwater Vision Profiler 5

UVP6 – Underwater Vision Profiler 6

OPC – Optical Plankton Counter

MOCNESS – Multiple Opening/Closing Net and Environmental Sensing System

VPR – Video Plankton Recorder

ZOOVIS – Zooplankton Visualization and Imaging System

SIPPER – Shadowed Image Particle Profiling Evaluation Recorder

LED – Light Emitting Diode

LIST OF APPENDICES

1. INTRODUCTION

1.1 THE ROLE OF COPEPODS IN THE NORTHWEST ATLANTIC OCEAN

Zooplankton are foundational to a productive marine or aquatic ecosystem. These microscopic animals are highly patchy and vary in distribution and abundance throughout the water column (Folt and Burns, 1999; Turner and Dagg, 1983). This distribution changes between day and night, as the zooplankton undertake diel-vertical migration which is a behavior to avoid visual predators in the surface layer during the day (Lampert, 1989). Thus, many zooplankters congregate at depth during daylight hours and migrate upward at night, either coming within metres of the sea surface or spreading throughout the water column, depending on species (Hays et al., 1994; Lampert, 1989). Zooplankton's role as an aquatic food source, along with the fact that many commercially important marine species spend a portion of their life as part of the planktonic community, highlights the importance of studying this group of animals.

Zooplankton support some of the largest filter-feeding megafauna via a short (and therefore energetically efficient) food chain (phytoplankton $\rightarrow$ zooplankton $\rightarrow$ predator). In the Northwest Atlantic, blue whales (*Balaenoptera musculus*) are specialist feeders on euphausiids (Gavrilchuk et al., 2014; Lesage et al., 2018). Fin whales (*Balaenoptera physalus*), sei whales (*Balaenoptera borealis*) and minke whales (*Balaenoptera acutorostrata*) feed on euphausiids along with small forage fish (Gavrilchuk et al., 2014; Johnston et al., 2005; Prieto et al., 2012; Woodley and Gaskin, 1996), while humpback whales (*Megaptera* novaeangliae) primarily target the small forage fish (Gavrilchuk et al.,

2014). All of these whale species also feed to some extent on copepods, which are the most prolific marine zooplankton taxon. These small crustaceans are the most abundant multi-celled organisms on Earth (Richardson, 2008; Schminke, 2007) and serve as a primary prey and lipid source for many consumers such as commercial fish species (Richardson, 2008; Runge, 1988) and megaplanktivores including the endangered basking shark (*Cetorhinus maximus*) and baleen whales such as the critically endangered North Atlantic right whale (*Eubalaena glacialis*) (Pershing and Stamieszkin, 2020; Sims and Merrett, 1997). Calanoid copepods make up the majority of the diet of basking sharks, right whales, and bowhead whales, who seek out patches with high densities of large, late-stage, lipid-rich calanoid copepods in the genus *Calanus* (Baumgartner et al., 2003; Pomerleau et al., 2014; Sims and Merrett, 1997).

Sightings of some of these megafauna species have declined in the Gulf of Maine and surrounding areas over the last decade or so, with the North Atlantic right whale nearly abandoning their summer feeding grounds in Grand Manan Basin (Hoogenboom et al., 2015; Meyer-Gutbrod et al., 2021). This marked decline in predator sightings has been attributed to a reduction in their copepod prey, driven by changes in the climate in this region (Davies et al., 2015; Meyer-Gutbrod et al., 2021; Record et al., 2019). Deep water in the Gulf of Maine has been warming at an accelerating rate, which has led to a decrease in the abundance of *Calanus finmarchicus* in this region (Meyer-Gutbrod et al., 2021, 2018; Meyer-Gutbrod et al., 2022; Record et al., 2019). More specifically, these warmer temperatures have led to a slowing of the advective processes that supply the Gulf of Maine with *Calanus*-laden source waters (Meyer-Gutbrod et al., 2021; Record et al., 2019). Models suggest that increasing ocean temperatures may reduce lipid stores in *Calanus*, leading to a reduced diapause period and smaller body size (Wilson et al., 2016).

Body size has been shown to have a positive relationship with lipid content (i.e. energy content) of copepods (Helenius et al., 2024) and therefore changes in the populations of zooplankton have energetic consequences for their predators (Chust et al., 2014). If ocean temperatures continue to warm, *Calanus finmarchicus* populations on the U.S. Northeast Continental Shelf, including the Gulf of Maine, are projected to decline by up to 50% by 2081-2100 (Grieve et al., 2017).

Calanoid copepods are bottom-up drivers of many marine food webs, including those that exist in the Gulf of Maine (Pershing and Stamieszkin, 2020). Understanding their population distribution and ecology is important for managing the species that support various industries in the area, such as tourism (e.g. whale watching) and fish harvesting. Changes in planktonic communities occur over various time and spatial scales, from days to decades and from metres to kilometres. Continuous, fine-scale monitoring of copepods and their environment could help capture changing dynamics to explain patterns we see in taxonomy, distribution, abundance and behaviour in both copepods and their predators, which are parameters that help inform management practices.

1.2 MONITORING ZOOPLANKTON COMMUNITIES

1.2.1 Ship-based sampling

Physical samples of zooplankton are collected using the ship-based deployment of nets, pumps and the Continuous Plankton Recorder (Continuous Plankton Recorder Survey, United Kingdom), which captures plankton in surface waters on sheets of silk, operated during shipboard cruises. Pumps and nets collect physical samples that are

followed up with microscope analysis or, more recently, benchtop imaging analysis (see Section 1.2.2). This method of sampling zooplankton is considered the gold-standard because ship-based collection of physical samples allows for identifying plankton to the highest possible taxonomic resolution (Giering et al., 2022), including sex and developmental stage. This type of information is important to understand species diversity, population dynamics, abundance, and distribution as they relate to the marine ecosystem. Zooplankton and water samples needed for biochemical studies and genetic sequencing can also only be collected using physical samplers. These types of instruments can collect discrete samples or samples that are integrated horizontally or vertically. However, the vertical resolution of nets is often too coarse (integrating over 10s of metres) to answer questions regarding variation in zooplankton concentration at the fine scale. Pumps can achieve high vertical resolution, and the Continuous Plankton Recorder (CPR) (Batten et al., 2003) which is towed behind commercial ships to continuously collect plankton at the surface across entire ocean basins, can collect fine scale horizontal samples. However, processing physical samples is resource-intense. Resource limitation means that continuous sampling using ships is not widely practiced, leading to the under-sampling of zooplankton communities.

Fine-scale vertical resolution of zooplankton can be achieved with less resource intensity by the use of sensors, which are typically able to collect data on the scale of < 1 metre. Some popular types of sensors include optical, acoustic, and imaging sensors, each with their own set of advantages and disadvantages (Lombard et al., 2019; Wiebe and Benfield, 2003). Typically, a suite of instruments comprising both physical collection tools and fine-scale sensors are needed to achieve high resolution of both the taxonomic composition and vertical distribution of the zooplankton community.

1.2.2 Plankton imaging systems

Recent advancements in plankton imaging technology have begun to transform the way we conduct plankton distribution studies. Cameras mounted on dissecting microscopes have been used for obtaining images to be archived for later measurements, including oil-sac volume of copepods (Miller, 2000; Tarrant et al., 2008), prosome length and width (Tarrant et al., 2008), and measurements of very small body parts like the jaw (Tarrant et al., 2014). This method for measurement offers the advantages of imaging live animals and creating an archive of animals that does not change through time. Plankton imagers that are separate from a benchtop microscope are newer technology that can resolve the taxonomic composition of the zooplankton community (although usually to a coarser level than is possible with traditional benchtop microscopy), and can capture important information such as interaction among organisms, behaviour, and even dormancy (Ohman, 2019). Images from such imaging sensors can also be important outreach tools to engage the public in zooplankton research (Pollina et al., 2022; Robinson et al., 2017). The first attempts at imaging plankton without a microscope began in 1979 (Ortner et al., 1979), and today, plankton imagers can be coarsely divided into benchtop and *in-situ* imagers (Martin-Cabrera et al., 2022).

Benchtop plankton imagers that process preserved plankton samples, such as the FlowCAM (Yokogawa Fluid Imaging Technologies, Inc., Scarborough, MA) and ZooScan (Hydroptic, France), can determine the taxonomic composition and abundance of preserved plankton samples using automatic classification in less time than it takes to yield this information with microscopy, although classifications are usually to a coarser level than is achievable with microscopy (Álvarez et al., 2014; Grosjean et al., 2004;

Sieracki et al., 1998a). However, these imagers process ship-collected, preserved samples and therefore face the same drawbacks that nets and pumps face in terms of coarse temporal and spatial resolution, and high costs associated with scientific research cruises. Additionally, taxonomic identification can be difficult in images if the animals are in an orientation that obscures identifying features or if species in the same genera can be separated only by looking at fine details under a microscope.

In-situ imagers are sensors that capture images of plankton in the ocean, typically without collecting a physical sample. Although the first *in-situ* imager that was tested used a net to help concentrate animals for imaging and collection (Ortner et al., 1981), *in-situ* imagers quickly proliferated into many forms of stand-alone devices (Wiebe and Benfield, 2003), including the Video Plankton Recorder (VPR) (Davis et al., 1992), the Underwater Vision Profilers (UVP) (Picheral et al., 2022, 2010), and the ZOOVIS (Bi et al., 2013). When co-located with net sampling, the VPR showed a similar taxonomic composition to the zooplankton community (with common taxa being proportionally similar within each instrument and rarer taxa being well captured by one instrument than the other, depending on the taxon) and comparable estimates of copepod concentrations (with the VPR overestimating by a factor of 2.9 due to net extrusion of small copepods) (Benfield et al., 1996). Conversely, another study found that the UVP5 underestimated copepod concentrations by a factor of 2 to 5 (Forest et al., 2012). All *in-situ* imagers can potentially undersample animals in the water column because the sampled volume in each image is small and many zooplankton show avoidance behavior to approaching platforms (Whitmore et al., 2019). *In-situ* imaging sensors can be mounted on shipboard profilers, which means they are restricted in time and space the same way net-collected samples are, or they can be mounted on autonomous platforms. Imaging systems allow fine-scale

sampling of zooplankton layers in the water column with minimal damage to sampled organisms and, like benchtop imagers, can be used to determine taxonomic composition (albeit at coarser resolution than from physical samples) and abundance.

Sampling rates of imaging devices are typically 1 Hz or higher, generating enormous imagery data sets very quickly. Processing imaging data requires the time investment of trained taxonomists to annotate imaged organisms with taxonomic information. This hurdle is being addressed by an ongoing, global effort to advance the automatic classification of plankton images using artificial intelligence (AI) systems. The first study to use machine learning for plankton imaging was in 1980 (Schlimpert et al., 1980) and since then, numerous groups have been advancing this area of research. AI can increase the efficiency of processing plankton image data while maintaining acceptable accuracy of taxonomic or morphological trait identification (Irisson et al., 2022) and estimations of lipid content from copepod constituents (Maps et al., 2024). This is done through the development of instruments and software that can automatically detect (Sieracki et al., 1998b) and classify regions of interest (ROIs) (Ellen et al., 2015, 2019; Gorsky et al., 2010; Schröder et al., 2020). Accuracy upwards of 80% has been achieved for taxonomic identifications and is highly dependent on the number of classifications the model can give (i.e., a model with fewer classification categories is more accurate) (Irisson et al., 2022).

The efficiency of using machine learning on *in-situ*-collected zooplankton images is sometimes hindered by an abundance of marine snow (i.e. particles of organic matter) in the water column, which can cause problems with the image segmentation part of classification (Bi et al., 2015; Ohman et al., 2019). In the present study, which was conducted in high-productivity coastal waters, there was concern that phytoplankton

blooms could lead to high marine snow concentration in the water column, potentially (1) obscuring identifying features of the animals in the images and leading to a lower taxonomic certainty even when using manual validation, or (2) completely obscuring animals, leading to them not being counted towards the total concentration. In the outer Bay of Fundy, peak phytoplankton abundances occur between spring and fall, although there is considerable year-to-year variation in timing of bloom and species composition (Martin et al., 2009).

After 40 years of advancement, the consensus among the zooplankton community is that imaging is an important part of monitoring zooplankton, but that there is further work to be done before imaging data alone can be trusted without being guided by net-sampling + microscopy (Giering et al., 2022). Additionally, machine learning for plankton requires local training datasets that were acquired with the same equipment as the test dataset [Frédéric Maps, Université Laval, pers. comm.], as photo libraries are non-transferrable between imagers, and no shadowgraph zooplankton image dataset exists yet for the Bay of Fundy region. This project is a contribution to the ambitious goal of yielding robust zooplankton datasets using autonomously collected imagery to help explain phenomena we observe in the marine ecosystem.

1.3 AUTONOMOUS UNDERWATER VEHICLES AND SENSORS FOR SAMPLING ZOOPLANKTON COMMUNITIES

Autonomous underwater vehicles (AUVs) refer to ocean-going platforms that are self-propelled and unmanned. This allows them to be deployed in all weather conditions

and in difficult-to-reach areas such as under sea ice (Sahoo et al., 2019). A ship may only be required for deployment and recovery. While deployed, AUVs are piloted remotely from a shore station using satellite communications.

Gliders are a type of battery-powered AUV that uses buoyancy generated by an air or oil bladder and lift generated via wings to control their position in the water column (Rudnick et al., 2004). Gliders survey along a programmed path by dead-reckoning using GPS fixes gained while at the surface. Their flight consists of slow, repeated dives in a saw-tooth pattern that results in efficient gliding (Deutsch et al., 2020), allowing for longer-term deployments (several weeks to several months) with continuous sampling (Rudnick et al., 2004).

Gliders can be equipped with a suite of sensors for sampling the ocean environment. Over the last several years, numerous research groups have begun experimenting with glider-mounted acoustic and optical zooplankton samplers. These sensors have been useful for measuring environmental variables (Benoit-Bird et al., 2018; Ruckdeschel et al., 2020), obtaining abundance estimates of zooplankton (Ohman et al., 2019; Reiss et al., 2021; Whitmore et al., 2019), and even studying the behaviour of some zooplankton (Guihen et al., 2022; Ohman, 2019). Glider-mounted imaging sensors have been able to provide quantitative estimates of many zooplankton, although this varies with taxa. Reiss et al. (2021) found that their glider-mounted echosounder gave higher concentration estimates of krill relative to ship-based samplers and attributed this to oversampling in areas where the glider was "stuck" in the currents. Whitmore et al. (2019) also found higher concentrations estimates measured with the Zooglider than associated net samplers, however these higher estimates were restricted to specific taxa that typically experience net extrusion and/or suffer from preservation artifacts (i.e. small copepods and

gelatinous zooplankton). Overall, sensor performance studies are in general, lacking, with no glider-based estimates of zooplankton abundance made in the Gulf of Maine using imaging sensors. This is a new and developing field of research that is being enabled by engineers who are designing energy-efficient sensors. There are some parameters that could affect the ability of imaging gliders to achieve sustained, quantitative monitoring. For example, imaging sensors are particularly power-hungry, and power draw could shorten the deployment time of battery-powered underwater platforms. Ship-mounted profilers are typically towed at ~1 m sec^{-1} through the water to minimize avoidance of the sampling tunnel by mobile plankton, but gliders can only achieve a descent rate of ~ 20 cm/sec. Ultimately, the combination of imaging sensors and autonomous platforms could allow for high time-space resolution of zooplankton communities over long time periods at a lower cost compared to ship-based sampling, enabling more accurate monitoring of these highly variable animals.

1.4 RESEARCH OBJECTIVES

The objective of my master's thesis is to evaluate a prototype, glider-mounted shadowgraph camera's ability to accurately measure zooplankton abundance, vertical distribution and taxonomic composition while deployed in the ocean. First, I wanted to compare the taxonomic capabilities of my sampling instruments (a glider-mounted shadowgraph camera, a MultiNet Midi, and an Underwater Vision Profiler 6-HF), particularly in their ability to collect images that can be used to accurately identify copepods and then be used to generate vertical profiles of copepod concentration. I also wanted to determine if higher marine snow in the water column affects the ability of the

imaging sensors to collect images that can be used to achieve the same certainty of taxonomic identification of ROIs, or the overall detectability of ROIs, taken under lower particle load conditions. Lastly, I wanted to determine if shadowgraph imagery is able to resolve zooplankton layers in both day and night. This would determine if diel-vertical migration is occurring in the dominant copepod taxa, where I would expect to see the highest concentrations of copepods deeper in the water column at day and move toward the surface at night.

The evaluation was accomplished by conducting an *in-situ* gear comparison study. The shadowgraph data was compared with co-located data collected with net samples and the UVP6. The shadowgraph camera I used is a prototype and, based on my observations using the camera in the field, I made modification recommendations to the manufacturer that can optimize the instrument for sustainable use in future ocean applications.

2. METHODS

2.1 SAMPLING EQUIPMENT

2.1.1 Shadowgraph camera mounted on a Slocum profiling electric glider

The glider used in this study was a G3 Slocum glider (Teledyne Webb, Massachusetts) (Schofield et al., 2007). It was a battery-operated, profiling electric glider equipped with a 200-metre buoyancy engine and a conductivity-temperature-depth (CTD) sensor. Maximum sampling depth was determined by constraints of the buoyancy engine pressure rating of 20 atmospheres, which equates to 200 metres depth in this study (buoyancy engines can be designed to accommodate pressures to 100 atmospheres or 1000 metres depth, and are swappable). In-water flight is mechanically controlled via the buoyancy engine, wings and a rudder at the tail-end of the glider. Gliders are far slower-moving than shipboard profilers, typically traveling at 0.5 km/h over ground and 10 to 20 cm/sec vertical profiling speed. The nose of the glider has a wet payload bay equipped with a downward-looking altimeter to sense distance from the seafloor or other possible obstructions. It will automatically ascend if obstructions have been detected below it.

The shadowgraph camera (Williamson and Associates Technologies, Seattle, WA) was mounted on the nose of the glider and electronically connected to the glider through waterproof cabling in the wet payload bay. This connection provided power to the camera during flight and allowed the camera to be programmed via the glider's science computer. The shadowgraph-glider set-up can be seen in Figure 1.

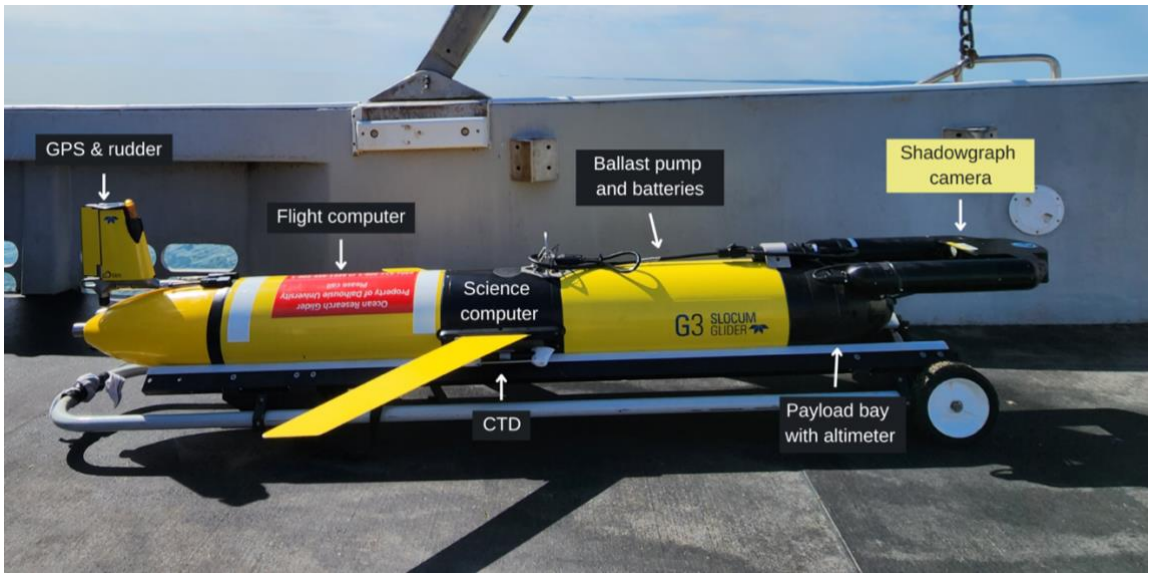

Figure 1. A Slocum G3 glider with a mounted shadowgraph camera.

The camera consists of two cylindrical pressure housings separated by an imaging tunnel (Figure 2A). The imaging tunnel measures 14.4 cm across its mouth where animals are considered in-focus across the entire volume of water due to the telecentricity of the camera (Figure 2C). When activated, the tunnel is illuminated from a red light-emitting diode (LED) bulb in the right-hand housing (Figure 2B). After passing through a plano-convex lens that collimates the light, it is reflected off a 45° mirror at the top of the housing and directed into the imaging tunnel. As zooplankton pass through this imaging tunnel, they interrupt the light path, creating a silhouette. The light around each silhouette is then received through the viewport on the left-hand side of the imaging tunnel, reflected off a 45° mirror, and through another plano-convex lens that focuses the light on the telecentric lens where the image is taken. The shadowgraph camera pixel resolution is approximately 17 μm.

Exposure and file settings for the camera were chosen with the goal of preserving image quality while imaging potentially fast-moving copepods in a moving fluid, which requires a higher shutter speed than for stationary objects. Prior to my field experiment, I undertook lab tests in a flume, and a functional check-out dive in Bedford Basin, Nova Scotia, to find the optimal settings for this goal (Table 1). In the flume, the shadowgraph was mounted in a relatively stationary position in the tank, such that it could neither move forward or backward, with the flow speed at ~20 cm/sec (the estimated speed that the glider would travel at on regular deployments, based on speeds obtained on previous deployments in the lab's research program). Preserved and/or live plankton samples were fed through the imaging tunnel. The camera was programmed with different exposure and capture settings like timelapse interval, total number of images to be taken, resolution of the photos, red and blue gain, ISO, frame rate, and file type and name for storage of the images (~57 combinations). The four settings combinations that were most optimal in the lab were then tested during the functional check-out dive (ISO 800 and shutter speeds 150, 200, 400, and 640 microseconds), and the settings which yielded the highest quality photos upon visual inspection were chosen to use in the field deployments (Table 1). During Bay of Fundy deployments, a test of the exposure settings with a slightly reduced shutter speed of 400 microseconds showed a more desirable contrast in the photos, so this shutter speed was used during the last day/night cycle of the experiment.

Table 1. Image and file type settings for the shadowgraph camera during deployments in the Bay of Fundy. All settings remained the same throughout the experiment with the exception of shutter speed (see main text).

File type	PNG
ISO	800
Shutter speed (September 8th & 11th)	640 microseconds
Shutter speed (September 19th)	400 microseconds
Image Resolution	4056 x 3040 pixels
Red gain	0.8
Blue gain	0.8
Monochrome on/off	On

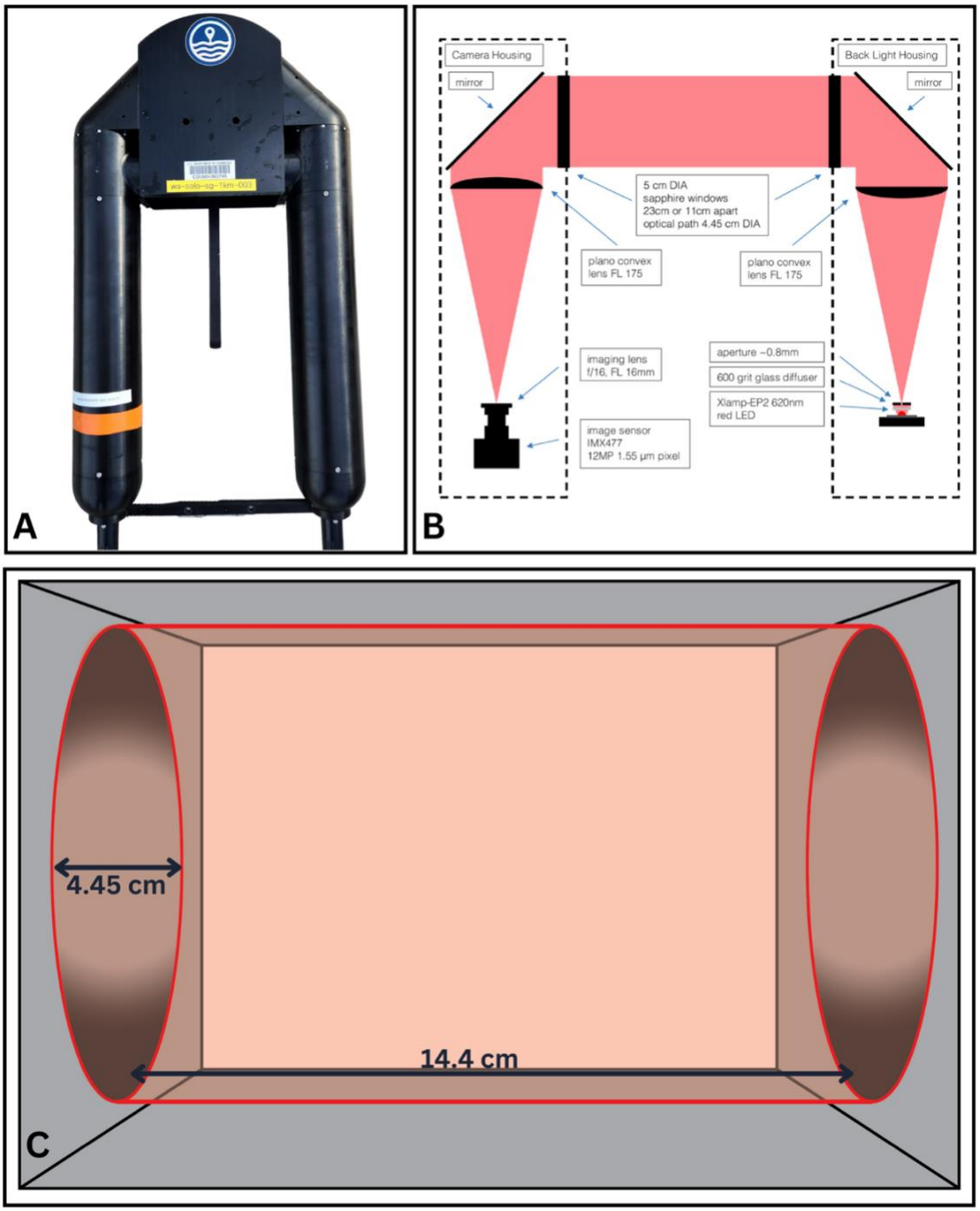

Figure 2. A) Shadowgraph camera housing. Each cylinder protects the electrical components of the shadowgraph camera system. B) A diagram of the inner components of each housing (reproduced with permission from the instrument manual written by

Williamson and Associates). C) The shadowgraph camera imaging tunnel. The imaged area is represented by the red cylindrical area.

The desired sampling rate was 1 Hz but during the first deployment cycle of the field experiment (see Section 2.2) it was discovered that, due to a hardware limitation inside the camera, this high sampling rate could not be sustained over the entire period of a dive. To achieve the highest sampling rate possible for the remainder of the study, the camera was programmed to sample "as fast as possible" in burst mode upon recommendation by the manufacturer. An approximate sampling frequency of 0.8 Hz was achieved. The final sampling rate setting used during the field experiment (Section 2.2) is listed in Table 2.

Table 2. Shadowgraph sampling rate settings for each day/night cycle in the Bay of Fundy. The image acquisition settings consist of an image sampling frequency, the number of photos to be taken, and whether or not the light is turned on for the photo. In this study, the light was on for every photo. See section 2.2 for details on the dates and station numbers associated with the field experiment.

Date	Stations	Frequency Setting	Number of photos
September 8th 2022 (practice cycle)	002 - 003	1 Hz (set, but not achieved due to hardware limit)	to capacity (actual #: 678)
September 8th 2022 (practice cycle)	004 - 007	maximum (~0.8 Hz*)	to capacity (actual #: 10,314)
September 11th 2022 (Cycle 1)	008 - 013	maximum (~0.8 Hz*)	to capacity (actual #: 14,858)
September 19th 2022 (Cycle 2)	014 - 019	maximum (~0.8 Hz*)	to capacity (actual #: 16,107)

** This frequency was calculated by dividing the number of photos taken during a dive by the time of the dive in seconds. This frequency was converted to Hz. The fractional sampling rate could not be determined (i.e. photo timestamps were not reported with miliseconds).*

2.1.2 Ground-truthing instruments: MultiNet Midi and Underwater Vision Profiler 6 (UVP6)

Two instruments were deployed from a ship using a winch and tow cable to collect ground-truthing data. The MultiNet Midi (Hydrobios, Germany) is a multiple opening-closing net system used to collect biological zooplankton samples (Figure 3). This plankton sampler has five 200 μm nets each mounted on a separate spring-loaded metal bar inside a frame with a $0.25m^2$ opening. There is an inner and outer flowmeter to measure the volume of water filtered at a 1 Hz sampling rate. Each net is programmed to open and close sequentially at desired depths using the pressure sensor in the instrument. All nets are closed and the spring-loaded bars locked in place when the instrument enters the water and on the downcast. The instrument descends until it reaches its pre-programmed unlocking depth, which unlocks the net opening mechanism. The winch then pulls the instrument up, and the MultiNet then begins its ascent. Once net 1's programmed pressure set-point has been reached, the lock on the bar for net 1 is released, the spring-loaded bar drops, and the net opens. When the pressure for net 2 is reached, the bar for net 2 drops, simultaneously closing the opening to net 1. This process is repeated for all 5 nets with the 5^{th} net remaining open until the surface. The MultiNet was deployed vertically and recovered at a towing speed of approximately 1 m/sec. Samples were filtered through a 210 μm sieve on deck to facilitate the transfer of biological material from the net to the sampling jar. All samples were preserved in 10% buffered formalin.

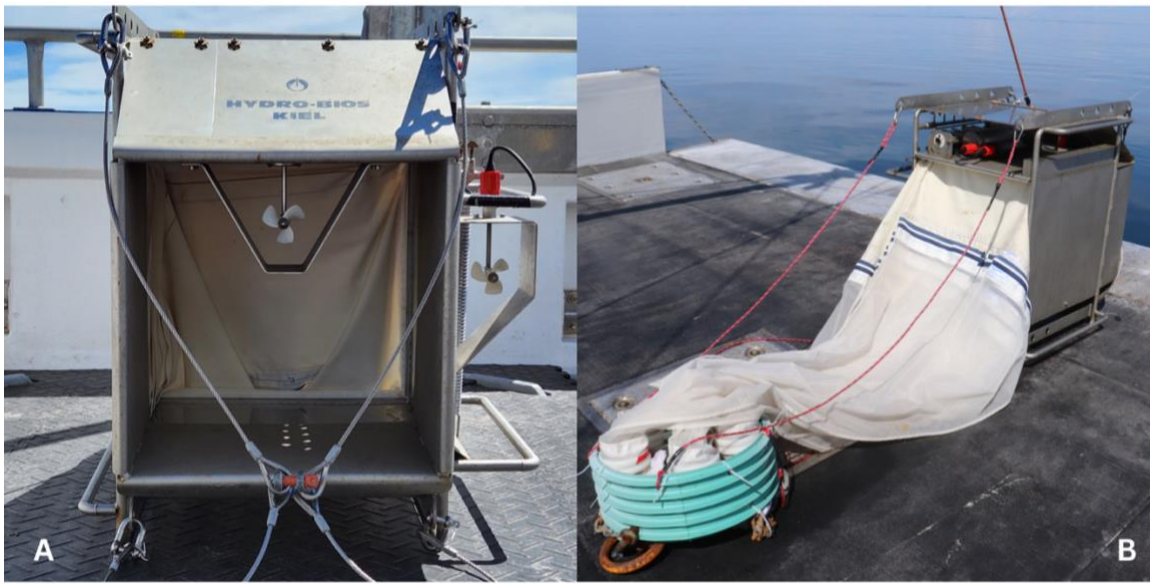

Figure 3. The MultiNet Midi (Hydrobios, Germany), a multiple opening-closing net plankton sampling instrument that allows the collection of depth-stratified samples. A) view through the frame opening where the inner and outer flowmeters are situated B) the sampling set-up for vertical tows. All cod-ends are secured to a weighed PVC "frame" to ensure the nets stay below the frame and the flow of water through the nets remains unobstructed.

The second instrument is the Underwater Vision Profiler 6 (UVP6, Hydroptic, France). Version 6 is the newest model of this optical plankton measuring device that has been widely used since the 1980s, and is a global industry standard device for *in-situ* particle measurements from images (Picheral et al., 2022). It consists of a camera, a light source, and a battery. The light source illuminated a 0.680-litre volume in front of the camera, where photos were acquired against a black background (Figure 4). The area illuminated varies slightly around 0.7 L depending on the factory calibration that is

specific to an instrument, and our instrument was calibrated to a 0.680 L sampling volume per image for this study. From each image, the *UVPapp2.2* (Hydroptic) software created separate image files of regions of interest (ROIs) and provided particle size and abundance information for all particles measured by the instrument. It retains images of any ROIs > 620μm in size, which users validate to obtain taxonomic information (see more in Section 2.4). This instrument was deployed and recovered vertically at a towing speed of approximately 1 m/sec, and it sampled at a rate of 5 Hz.

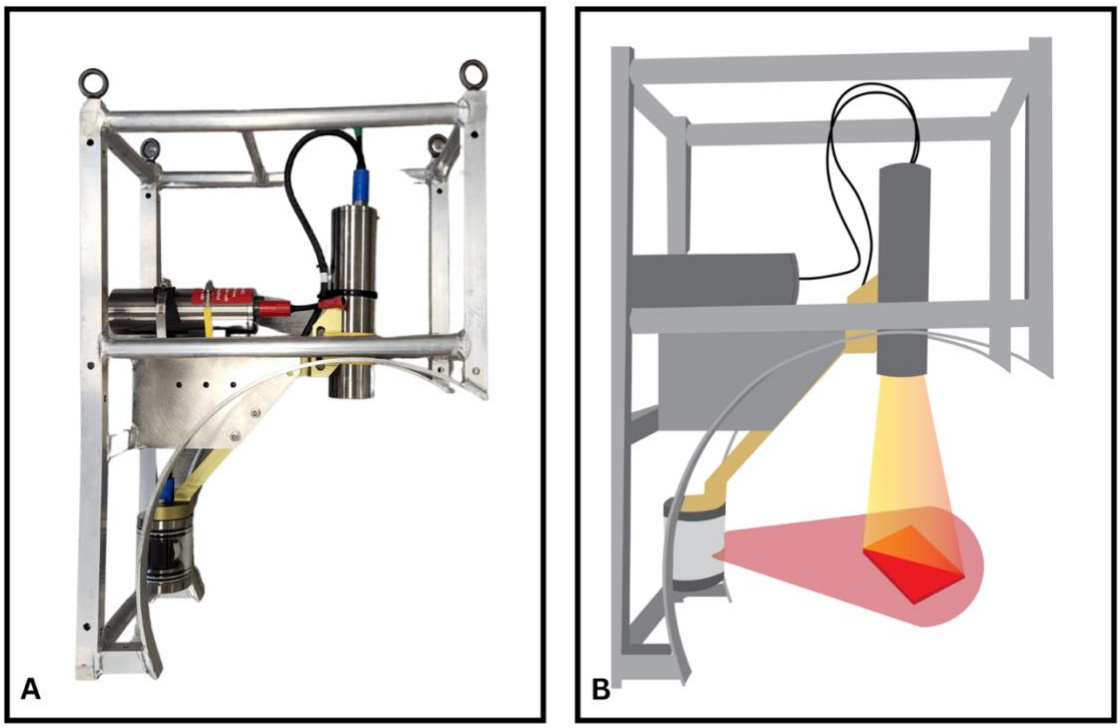

Figure 4. The Underwater Vision Profiler 6, a plankton imaging device that specializes in imaging large (> 620μm) particles. It consists of a camera, a battery, and a light source. A) the UVP6 set-up in its frame. B) a diagram of the image-taking process (reproduced from Picheral et al., 2022). The dark red area represents the imaged area.

2.2 GEAR COMPARISON STUDY

The field experiment for this study took place in Grand Manan Basin, the deepest part of the outer Bay of Fundy, Canada during September 2022. The glider was deployed from the manned research vessel and was programmed to descend to ~10m above the seafloor on a flight path near the 200 m depth contour. During deployment, it surfaced several times to obtain GPS data and reorient along the programmed path as needed. Using these GPS locations, we chose three stations along the glider's path at which to collect ground-truthing data. Each station consisted of a vertical MultiNet tow, followed by a UVP6 cast, followed by a CTD-mounted flurometer cast. The MultiNet's programmed depths split the water column up into five, roughly-equal depth strata. This cycle was repeated during both day and night within a 24-hour period to account for any differences in the camera's ability to collect useful images under different light conditions, and also diel-varying zooplankton vertical distributions and behaviours. Two day-night cycles were conducted early in the month (September 8^{th}/9^{th} and September 11^{th}/12^{th}) and one later in the month (September 19^{th}/20^{th}). Glider transects and accompanying ground-truthing stations from September 11^{th}/12^{th} and September 19^{th}/20^{th} can be seen in Figure 5.

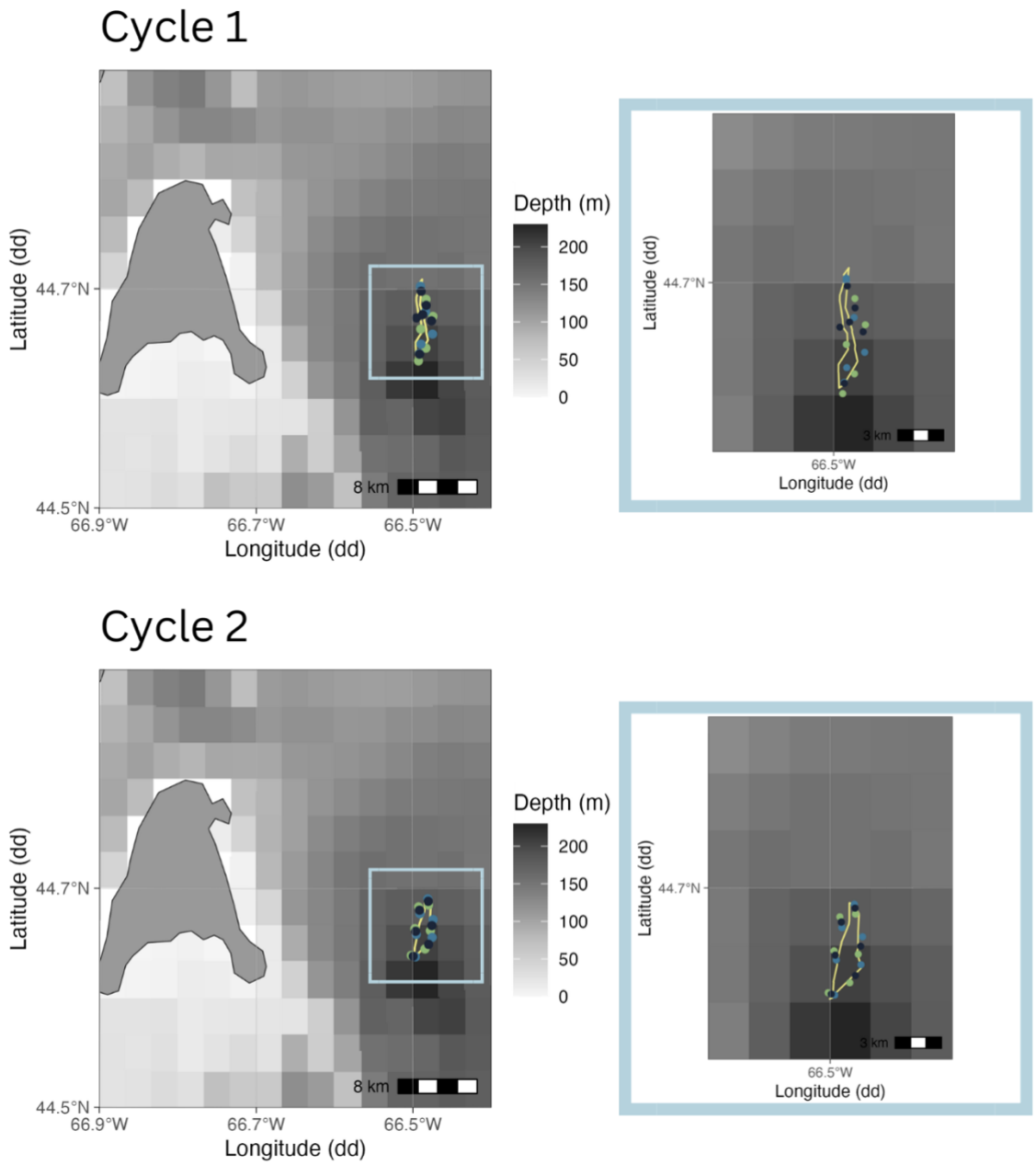

Figure 5. Glider transects for the day and night sampling during Cycle 1 (September 11th/12th) and Cycle 2 (September 19th/20th). The yellow line is the path of the glider, blue points represent a MultiNet tow, navy points represent a UVP6 cast, and green points represent a CTD cast.

2.3 DATA PROCESSING

2.3.1 *MultiNet*

Sixty out of 90 of the biological samples collected were analyzed to allow comparisons between bloom and non-bloom conditions while operating within reasonable time constraints. These were the samples collected on September $11^{th}/12^{th}$ (n=30) and $19^{th}/20^{th}$ (n=30) (Cycles 1 and 2). These cycles were chosen because they maintained relatively stable shadowgraph sampling rates, unlike the practice cycle conducted on September 8^{th}, which had a variable sampling rate due to a hardware limitation. A variable rate could bias estimates of copepod concentration downward in areas of the water column that were sampled at lower frequency, if much less water was sampled in some depth strata compared to others, so this cycle was deemed a "practice cycle" and was not included in the analyses of this thesis.

Processing of MultiNet samples to calculate zooplankton abundance and taxonomic composition followed a standard procedure developed based on a protocol used by Atlantic Reference Center (ARC; Huntsman Marine Sciences Centre, St. Andrews, NB). Macro-zooplankton (≥ 10mm) were first separated from each net sample by eye. These animals were enumerated separately from the meso-zooplankton (< 10mm). Zooplankton samples were then divided into subsamples using the HML beaker technique described in Van Guelpen et al. (1982). A split with 200 – 300 animals was taxonomically identified as finely as possible and enumerated. Additional splits were processed to identify only *Calanus* until at least 75 individuals were identified. This ensured that the abundance count of *Calanus* was more accurate, since this is the genus of primary interest

in the context of this research program. Developmental stages of the animals were noted where possible (copepodite stages I-IV, larva, cyprid, colonial, solitary, juvenile, egg, nauplius, calytopis). As a standard practice, the blotted wet weight of the meso- and macro- zooplankton were weighed separately to the closest 10^{-4} grams. A detailed description of this process is available in Appendix A.

2.3.2 Underwater Vision Profiler 6 (UVP6)

The UVP6 images particles on a black background, allowing the internal software of the instrument to segment the image based on pixel light intensity (Picheral et al., 2022). Within the imaged volume of water, all particles are considered to be in focus and at a known distance from the lens, enabling accurate size measurements of particles. While the size data of all particles are collected, only the ROIs of those measuring ≥ 620μm are retained for classification. The retained ROIs consist of zooplankton as well as marine snow. These data (particle counts and extracted ROIs) were imported into EcoPart and EcoTaxa, respectively (available at https://ecopart.obs-vlfr.fr/ and https://ecotaxa.obs-vlfr.fr/). These are web-based applications designed to work synergistically with data from UVPs. This software allows the user to look at ROIs as single images and assign an annotation to that image. I trained an undergraduate student to classify ROIs into taxonomic categories as finely as possible using the nomenclature available in the database (Appendix B). One hundred percent of the ROIs were annotated manually. Appendix B depicts all of the identifications made in the project. However, some identifications may not be represented in the analysis because some taxa were aggregated

and some images that were collected were not used in the inter-instrument comparison analysis. Images were excluded from inter-instrument comparison if they occurred below the deepest sampling depth of the MultiNet, or if they occurred while there was still influence from the sun at the surface. Identifications were also assigned a categorical group of definite or possible which corresponded to the certainty in the identification. Meristic and morphometric traits such as presence or absence of legs, urosomes, antennae, egg sacs, muscle bands, meridional canals, as well as general body shape and size were used to determine to which certainty category each ROI belonged. Identifications are somewhat objective and a combination of traits were used to identify an animal depending on what traits were available to evaluate in each ROI. Some example ROIs of the taxa found in the UVP6 images can be seen in Figure 6.

In addition to taxonomic identification of animals, marine snow particles were annotated. This allowed deterimnation of the concentration of marine snow particles throughout the water column separately from the animals, as the particle data from the instrument could contain both marine snow and animals.

2.3.3 Shadowgraph Camera

Shadowgraph data from glider profiles associated with Cycles 1 and 2 were analyzed for this thesis. Photos were annotated using the application Video and Image Analytics for Multiple Environments (VIAME, available at https://github.com/VIAME/VIAME) by drawing a box or outline around each ROI and assigning an identification. All ROIs were detected and annotated manually. Annotations in this project can be seen in Appendix C and, like the UVP6, some identifications may

not be represented once data were aggregated or trimmed for inter-instrument comparison. Images excluded from inter-instrument comparison included those that occurred below the deepest sampling depth of the MultiNet and those that occurred during profiles that were not most closely aligned in time and space with a MultiNet tow. These identifications were also assigned a certainty category of definite or possible in a similar fashion to the UVP6 method. VIAME allows whole images to be analyzed to assign annotations to multiple ROIs in a single image. This software was used instead of EcoTaxa, which is an industry standard, because the experimental nature of the instrument and the project means the pipeline to extract ROIs of a specific size and prepare for import into EcoTaxa does not yet exist, whereas our collaborators have been building a VIAME application for our camera. One advantage of using VIAME is that it allowed analysts to manually identify ROIs that contain our target taxa (i.e., zooplankton) without the need to sort through ROIs that EcoTaxa has assigned as important but that are not targets of this study (i.e., marine snow).

The glider downcasts that most closely aligned with the MultiNet in time and space were chosen for inter-instrument comparison at each station. The complete profile consisted of the first photo the glider took upon descent to the last photo taken at its deepest depth. For most profiles, a mismatch in the glider's dive initiation and the shadowgraph's photo acquisition initiation meant that the first ~9 metres of the water column were not imaged. Some example photos of the taxa found in the shadowgraph images can be found in Figure 7.

2.4 DATA AND STATISTICAL ANALYSIS

2.4.1 Concentration calculations

Copepod abundance counts for all instruments contain animals classified as Copepoda. Copepod concentration estimates from the MultiNet (C_{net}) were derived from the abundance counts (which contain all individuals under Copepoda) obtained from the biological samples and adjusted for the flow of water through each net, measured via the MultiNet's inner flowmetre. Notation for this calculation can be seen in Equation 1:

$$C_{net} = \frac{individuals_i}{\sum_{j=1}^{n}(flow_{i,j}) \cdot net\ area\ opening} \qquad \text{(Equation 1)}$$

Individuals refers to the number of individuals in a taxon in net *i*, flow is the speed measured by the flowmeter in m/sec , which is summed over each 1-second time step *j* while net *i* was open between time steps 1 (at net opening) to *n* (at net closing), and the net area opening is in square metres (and for the MultiNet Midi is always 0.25m^2).

Copepod concentration estimates from the UVP6 (C_{uvp}) in each depth stratum are derived from abundance counts as obtained from image annotations and adjusted for the volume of water imaged in a given depth bin. Notation for this calculation can be seen in Equation 2:

$$C_{uvp,k} = \frac{\sum_{k=1}^{n} individuals_k}{\sum_{k=1}^{n} \#\ images_k\ .\ image\ volume} \qquad \text{(Equation 2)}$$

Individuals refers to the number of individuals in a taxon in the images in a given depth bin *k*, beginning at step 1 (start image) to *n* (end image), the number of images is the total collected within each depth bin *k* beginning at step 1 (start image) to *n* (end image, and image volume is the volume of water associated with each image (for the 2022 UVP6 calibration this is $6.8 \cdot 10^{-4}$ m^3). The summation of the number of individuals in a taxon in each image in a depth bin gives the abundance of a taxon throughout the whole depth bin. For statistical analysis, the depth bin used matched that of the corresponding MultiNet tow and net.

Copepod concentration estimates from the shadowgraph (C_{shadow}) are derived from abundance counts from annotated images and adjusted for the volume of water imaged in a given depth bin. Notation for this calculation can be seen in Equation 3:

$$C_{shadow,l} = \frac{\Sigma_{l=1}^{n} individuals_l}{\sum_{l=1}^{n} \#\, images_l \,.\, image\ volume} \qquad \text{(Equation 3)}$$

Individuals refers to the number of individuals in a taxon in the images taken in depth bin *l* beginning at step 1 (start image) to *n* (end image), the number of images is the total collected at each depth stratum *l* beginning at step 1 (start image) to *n* (end image), and image volume is the volume of water in each image (and for the shadowgraph this is $2.2396 \cdot 10^{-4}$ m^3). The summation of the number of individuals in a taxon in each image in a depth stratum gives the abundance of a taxon throughout the whole depth stratum. For statistical analysis, the depth bin used matched that of the corresponding MultiNet tow and net.

The volume in a single shadowgraph image ($2.2396 \cdot 10^{-4}$ m^3) was calculated for the illuminated cylindrical area in the image tunnel (Figure 2C). Notation for this calculation can be seen in Equation 4:

$$V_s = \pi(0.0445 \text{ meters}/2)^2 \cdot 0.144 \text{ meters} \quad \text{(Equation 4)}$$

2.4.2 Statistical analysis

Data were analyzed to determine the shadowgraph camera's ability to obtain accurate concentration estimates, using the MultiNet data as "true" concentrations in a depth bin. Therefore, concentration estimates from the various sampling instruments were compared within a depth bin corresponding to each MultiNet net. The analysis also aimed to understand if the shadowgraph could detect copepod layers in the water column (from approximately 10 metres above the seafloor to 9 metres below the surface) and if so, to what resolution compared to the MultiNet and UVP6. Since the MultiNet integrates animals over 10s of metres, I expected sensors to be able to detect variation in concentration within a depth of that range.

All day and night stations (consisting of a MultiNet tow, a UVP6 cast, and a CTD cast) in each cycle were paired with a shadowgraph downcast that occurred most closely in time to the MultiNet tow and these profiles were used for all analyses. At station 009, the glider incorrectly detected an obstruction below it and ascended before sampling the last two depth bins. These depth bins were excluded from further analyses. The taxonomic breakdown was compared across the three instruments to visualize which taxa the varying

instruments excelled at capturing and imaged well enough to be identified. Depth profiles were generated for taxa of interest (copepods and some gelatinous zooplankton). Descriptive statistics such as the average total copepod concentration per net and the average concentration of the major Copepoda constituents per net were determined. A Wilcoxon test between the net with the highest concentration and the nets with relatively lower concentration determined if the high-concentration layer was significant. Over- or under- estimation factors were generated by dividing the copepod concentration measured by the MultiNet by the copepod concentration measured by each imaging sensor and identification combination (definites-only or the sum of definite and possible identifications). The correlations between concentrations of copepods gained from the various instruments were evaluated using the Spearman correlation coefficient. Relationships were tested between the MultiNet and each imaging device using definite-only or the sum of definite and possible identifications. Additionally, the relationship between the UVP and shadowgraph was tested using definite-only or the sum of definite and possible identifications. The relationship between *Calanus finmarchicus* concentrations from the MultiNet data and *C. finmarchicus*-sized particles (1.6 – 2 mm) from the UVP6 data was also examined with a Spearman correlation coefficient.

To examine the effect of high marine snow concentration on taxonomic certainty, I analyzed one cycle early in the month (Cycle 1) and one cycle later in the month (Cycle 2) with the expectation that there would be varying bloom conditions between the two cycles, and that bloom conditions being correlated with higher marine snow concentration. To characterize the environmental conditions in each cycle, fluorescence concentrations were averaged over 5-metre depth bins across all stations in a given cycle. Those concentrations were then plotted against all marine-snow identifications from the UVP6

imagery in each cycle to examine this relationship. The ratio of definite to possible copepod identifications was calculated for each net combination that was inside (Nets 1 and 2) and outside (Net 3-5) the depths where the highest concentrations of marine snow occurred. Depth bins where the number of possible identifications was 0 were removed from this analysis. For each imaging instrument, a Wilcoxon rank-sum test determined if this ratio differed between areas of relatively high and low marine snow concentration. If the relative proportion of possible identifications increased under bloom conditions, I would conclude that higher marine snow concentration in the water column hinders our ability to use the imagery for accurate taxonomic identifications. Additionally, a Spearman correlation was used to examine this relationship on a continuous scale. To address the issue of complete obscuration of copepods by marine snow, the copepod concentration measured by each imaging sensor was subtracted from that measured by the MultiNet in each depth stratum to determine the "missed" concentration of copepods. This was then plotted against the concentration of marine snow in the same depth strata and a Spearman correlation was used to examine the relationship between the two concentrations. A strong, positive correlation would indicate a strong relationship between marine snow concentration and "missed" copepod concentration, leading me to conclude that higher marine snow concentration in the water column leads to under-inflated copepod concentration estimates when using imagery instead of net samples. The effect of high copepod concentration leading to masking of copepods by other other copepods was also evaluated with a Spearman correlation, with a strong, positive relationship indicating that the imaging sensors are not performing similarly under when sampling areas of high and low copepod concentration.

To examine diel-vertical migration of copepods, the effect of net number (i.e depth) and day/night condition were compared with a two-way ANOVA for C_{net}, C_{shadow}, and C_{uvp}. This test was also used to look at these patterns in *Calanus finmarchicus* in the MultiNet data. Only definite identifications were used for these comparisons because this removed the possibility that uncertain identifications would affect our results.

3. RESULTS

3.1 ACCURACY OF TAXONOMIC IDENTIFICATIONS AND CONCENTRATION ESTIMATES BY IMAGING SENSORS

The shadowgraph camera collected images of copepods and other zooplankton at all stations as expected, with one co-located dive ending before the glider reached the seafloor because it incorrectly sensed an obstruction. Examples of images taken with the shadowgraph are seen in Figure 6, and examples of images taken with the UVP are shown in Figure 7. Ninety percent of all animals identified in the MultiNet samples belonged to Copepoda, while 85% and 79% of animals measured by the shadowgraph and UVP6 belonged to the Copepoda, respectively (Figure 8). Animals in the imagery were rarely identifiable beyond the family level, whereas most animals in the MultiNet samples could be identified at least to genus level. However, in some cases, the imagery was able to be used to make finer identifications. Two copepod genera (*Calanus* and *Paraeuchaeta*) could be identified using the UVP6 imagery, although only in a couple instances each. Four genera were occasionally identifiable in the shadowgraph imagery (*Calanus, Paraeuchaeta, Oithona* and *Centropages*). Both instruments captured the annelid genus *Tomopteris* at least once, and the shadowgraph imagery was used to identify one ctenophore species to genus (*Beroe*) and another to species (*Pleurobranchia pileus*). This is the same level of identification made for these ctenophores using microscopy. Definite taxonomic identifications made by the UVP6 are found in Appendix B, Table 3 and those made by the shadowgraph are in Appendix C, Table 4. Estimates of proportion of salps in

the zooplankton community were similar between the MultiNet and the UVP6, with the majority of salps in the UVP6 imagery occurring during Cycle 1 (Figure 9). An interesting finding in the shadowgraph imagery was the capture of siphonophore larvae (siphonulae), which were imaged 112 times (Figure 10). The vast majority of these identifications occurred during Cycle 2. Figure 11 shows the vertical profiles of the larvae during Cycle 2, with the maximum concentration reaching 491 individuals m^{-3}. These larvae were not captured by either the MultiNet nor the UVP6.

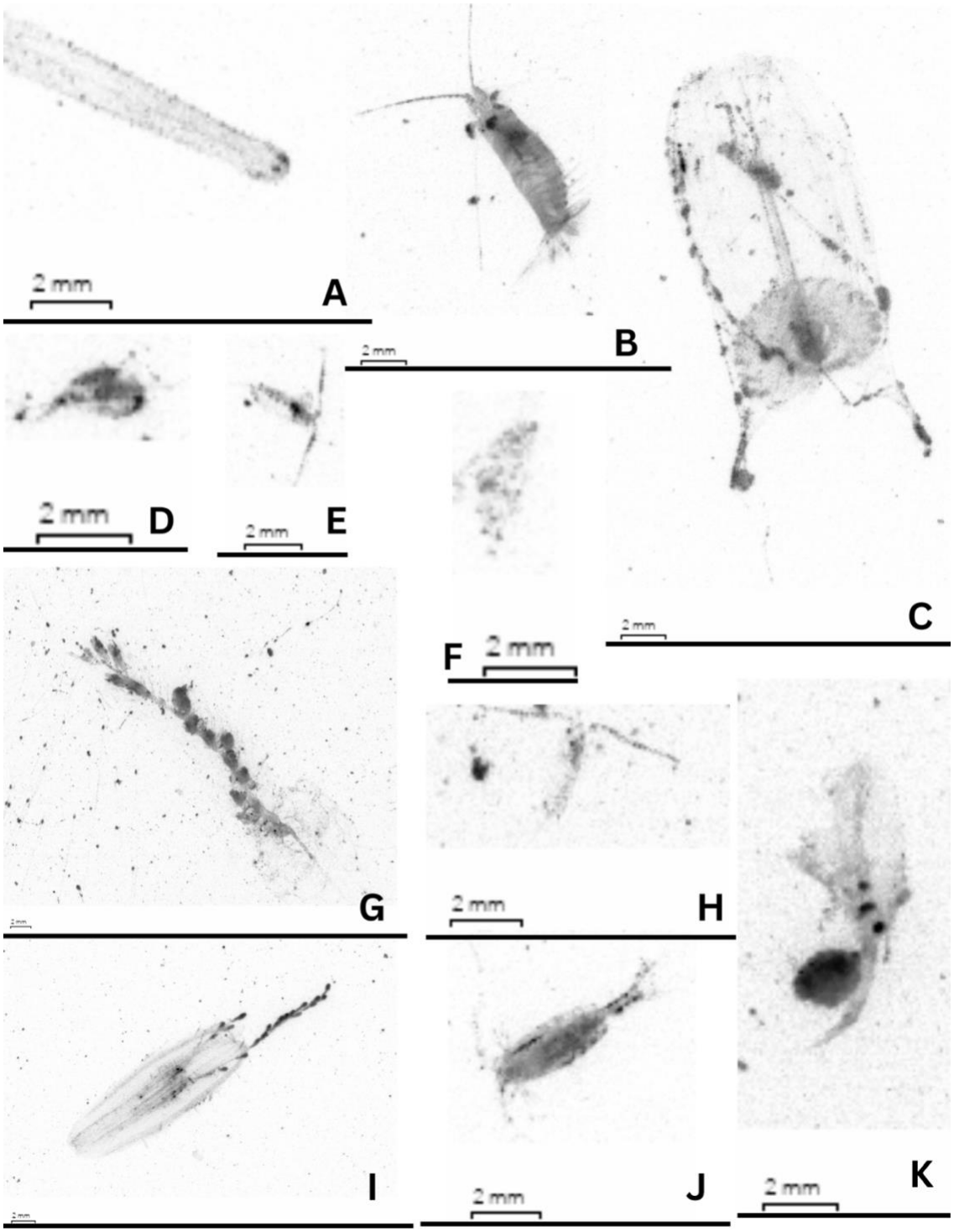

Figure 6. Example high-quality images of the taxa found in the UVP6 casts: A) Chaetognatha; B) Euphausiacea; C) Salpidae; D) Amphipoda; E, H & J) Copepoda; F) Echinodermata (larva); G) Siphonophorae; I) Ctenophora; K) Copepoda (with eggs).

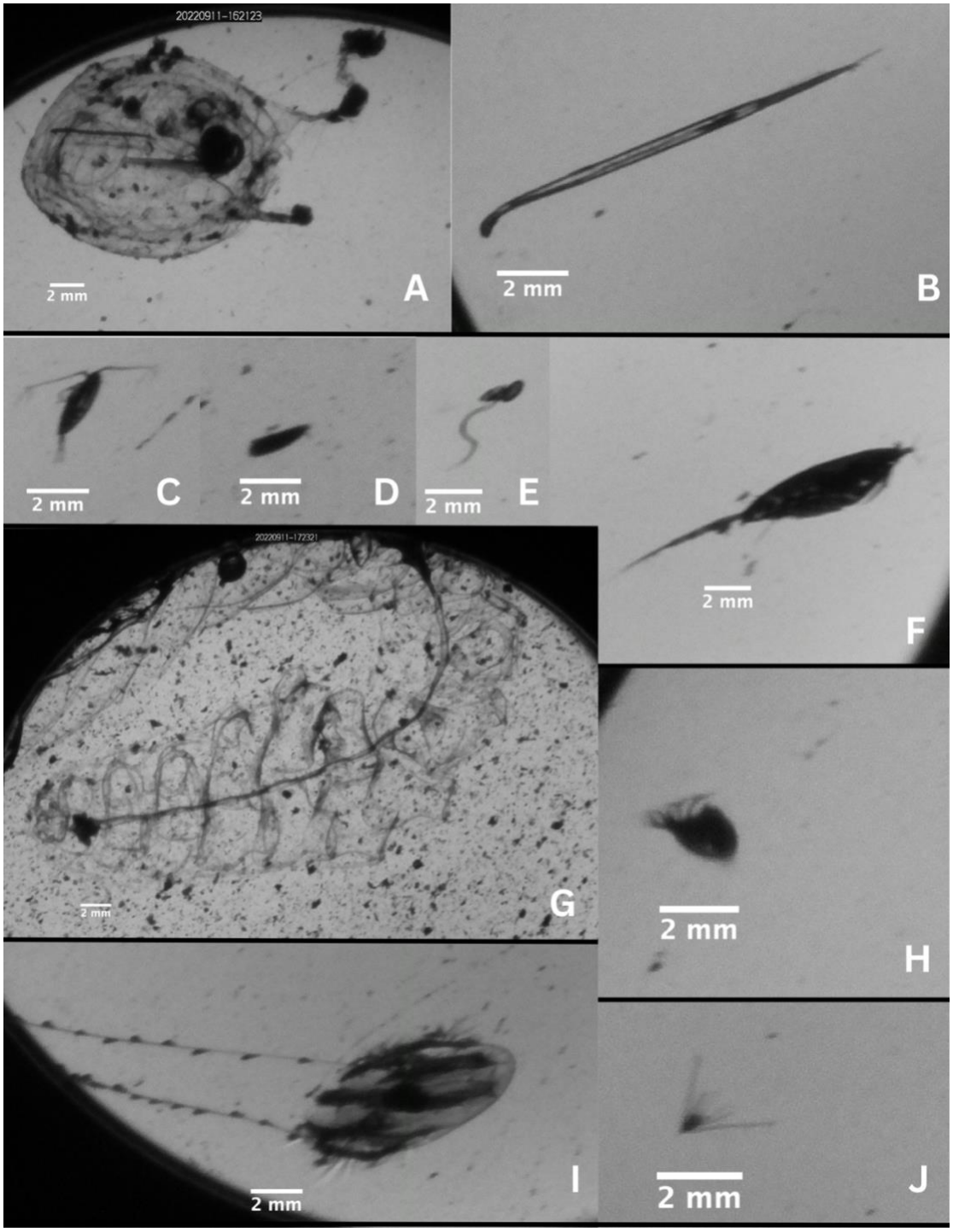

Figure 7. Example images of the taxa found in the shadowgraph profiles: A) Salpidae; B) Chaetognatha; C) Copepoda (general); D) Ostracoda; E) Appendicularia; F) *Paraeuchaeta* sp. (Copepoda); G) Siphonophorae; H) Amphipoda; I) Ctenophora; J) Echinodermata (larva).

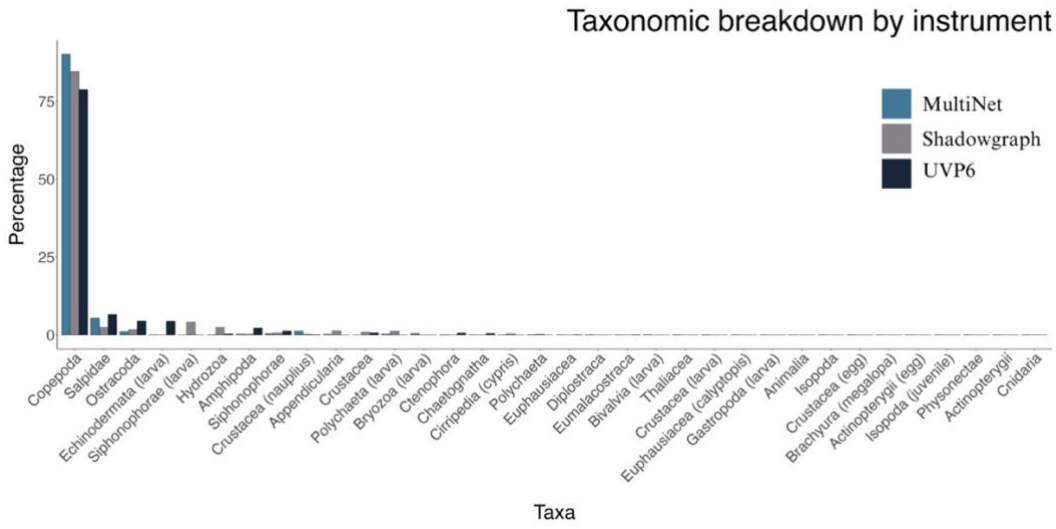

Figure 8. Bar plot comparing the relative percentage of each taxon measured by the three sampling instruments. MultiNet percentages are shown in blue, the UVP6 in black, and the shadowgraph in grey. All identifications shown here are definite-only.

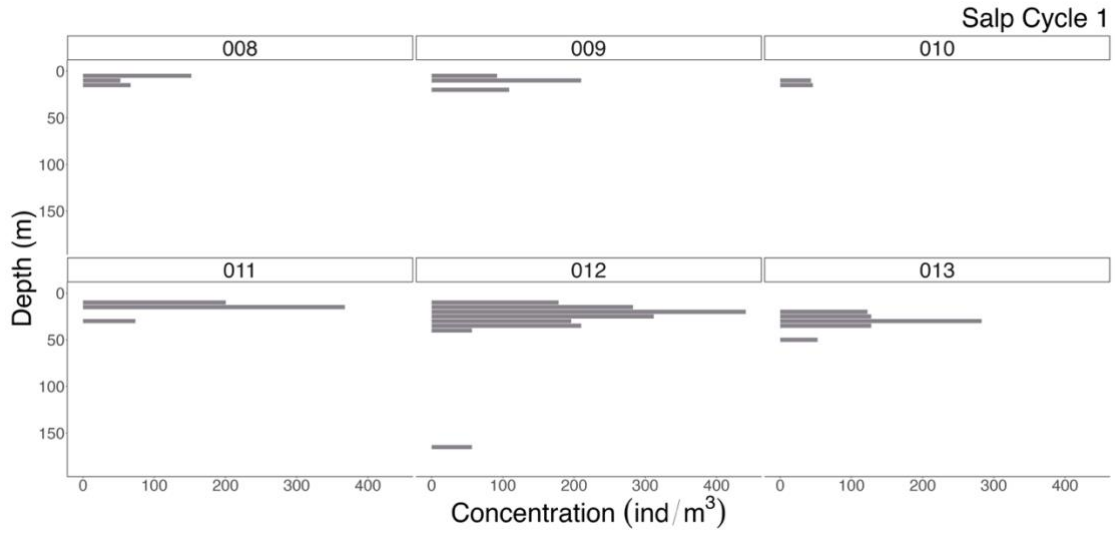

Figure 9. Vertical variation in total salp concentration (individuals m^{-3}) throughout the water column at each station in day (008-010) and night (011-013) for Cycle 1 as measured by the UVP6. These identifications are definite-only.

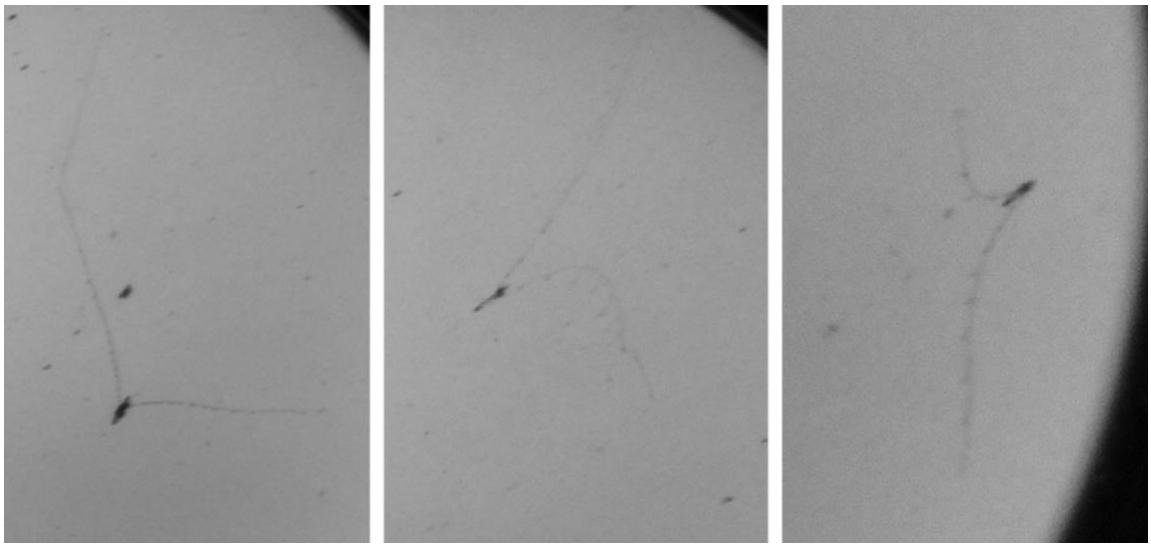

Figure 10. Example images of siphonulae (siphonophore larvae) captured in the shadowgraph imagery.

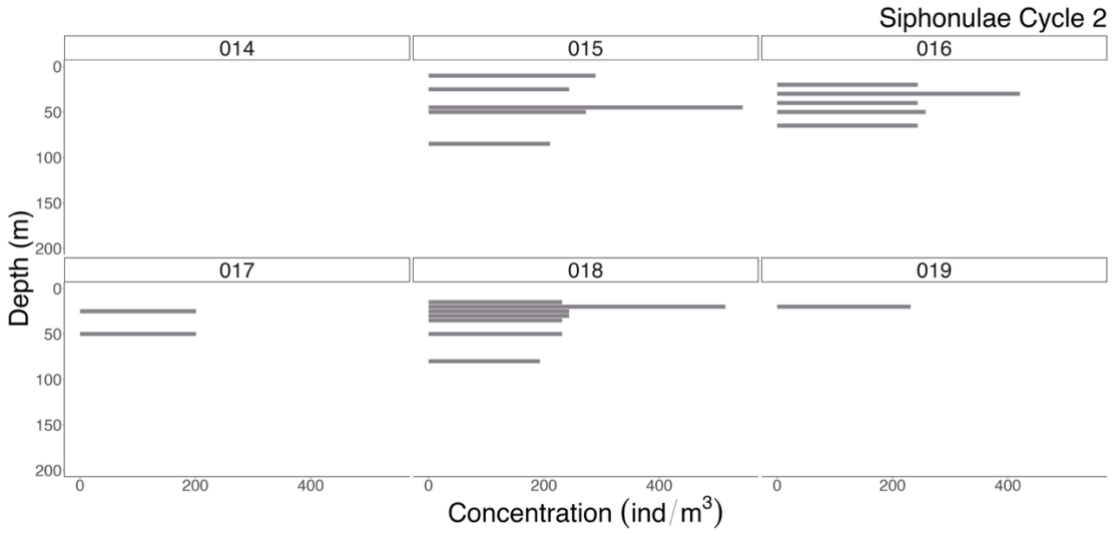

Figure 11. Vertical profiles of siphonulae concentration (individuals m^{-3}) throughout the water column at each station in day (014-016) and night (017-019) for Cycle 2 as measured by the shadowgraph. These identifications are definite-only.

The concentration of copepods varied throughout the water column. There was a strong and consistent copepod layer in the upper ~50 m of the water column and persisted in both day and night (Figures 12, 13), contrary to what it would be expected from a typical diel-vertical migration. Copepods were significantly more abundant at the shallowest depth across all stations and cycles as measured by the MultiNet (Wilcoxon, $p < 0.0001$, n = 60) (Table 5). The same was measured by the shadowgraph (Wilcoxon, $p < 0.0001$, n = 58) and the UVP6 (Wilcoxon, $p = 0.04$, n = 60) using definite-only identifications (Table 5). Visual inspection of the MultiNet taxonomic data showed that the layer in the shallow net consisted of a high abundance of adult *Centropages spp.* and *Oithona spp.* with lesser contributions of early copepodite stages of *Centropages, Paracalanus, Pseudocalanus and Clausocalanus* (Tables 6, 7).

Table 5. The average concentration ± SE found in two depth strata across the MultiNet, shadowgraph camera, and UVP6. Concentrations are reported in individuals m^{-3}.

Depth stratum	C_{net} (individuals m^{-3})	C_{shadow} (individuals m^{-3})	C_{uvp} (individuals m^{-3})
Nets 1-4 (deep ~35-175m)	410 ± 20	140 ± 10	80 ± 10
Net 5 (shallow ~0-34m)	3460 ± 530	820 ± 110	140 ± 30

Variation was also found in the concentration of *Calanus finmarchicus* throughout the water column (Figures 14, 15), with the maximum recorded concentration reaching 270 individuals m^{-3}. *C. finmarchicus* concentrations were typically highest in the midwater to deep nets. Overall, average concentrations were low, peaking in nets 2 and 3 with 190 ± 40 individuals m^{-3} and 190 ± 100 individuals m^{-3}, respectively, followed by net 1 at 140 ± 50 individuals m^{-3}, net 4 at 60 ± 20 individuals m^{-3}, and net 5 at 50 ± 10 individuals m^{-3}. These concentrations were negatively correlated with *Calanus*-sized (1.6 – 2 mm) particles measured with the UVP6 (Spearman, ρ = -0.33), although the relationship was significant ($p < 0.0001$, n = 60). Depth profiles of the overlapping concentrations can be seen in Figures 14 and 15.

Both imaging sensors underestimated total copepod concentration compared to the MultiNet (Table 6) with the shadowgraph concentration underestimating the net by a factor of 3-5. Because there was a higher underestimation in the shallowest layer where copepods were densest, I explored the idea that the difference in absolute copepod

concentration could be due to masking by other copepods. The correlation between the "missed" concentration of copepods with the imaging sensor and the copepod concentration measured with the MultiNet was strong for both the UVP and the shadowgraph (Figure 16).

Table 6. Underestimation factors ± SD of the MultiNet by each imaging sensor using definite-only identifications or the sum of definite and possible identifications. Estimates are given for overall concentrations and concentrations inside and outside of the layer present in the depth bin associated with net 5.

Instrument	Identification	Overall	Inside layer	Outside layer
Shadowgraph	Definite	4 ± 2 (n = 58)	5 ± 2 (n =12)	4 ± 2 (n = 46)
Shadowgraph	Definite + Possible	3 ± 2 (n = 58)	3 ± 2 (n = 12)	3 ± 2 (n = 46)
UVP	Definite	18 ± 45 (n = 60)	35 ± 29 (n = 12)	14 ± 48 (n = 12)
UVP	Definite + Possible	5 ± 7 (n = 60)	9 ± 4 (n = 12)	4 ± 7 (n = 12)

Table 7. Zooplankton species composition and average concentration (individuals m^{-3}) ± SE per net during Cycle 1. The depth range over which each net sampled is indicated. Net 1 represents the deepest depth bin of the MutliNet, and Net 5 represents the shallowest depth bin (n=6 per net).

	Net 1 (~144-175m)	**Net 2** (~107-143m)	**Net 3** (~71-106m)	**Net 4** (~35-72m)	**Net 5** (~0-34m)
*Calanus spp.**	171 ± 37	205 ± 45	179 ± 48	75 ± 31	57 ± 9
Centropages spp.	6 ± 4	2 ± 3	7 ± 4	71 ± 67	779 ± 343
Copepoda**	22 ± 9	8 ± 3	10 ± 7	44 ± 33	603 ± 239
Metridia spp.	35 ± 14	25 ± 7	25 ± 14	30 ± 9	24 ± 23
Microcalanus spp.	35 ± 14	68 ± 24	73 ± 25	14 ± 11	3 ± 7
Oithona spp.	56 ± 19	37 ± 13	39 ± 18	138 ± 86	644 ± 308
Paracalanus spp.	2 ± 3	0 ± 1	4 ± 4	23 ± 23	184 ± 41
Pseudocalanus spp.	10 ± 5	7 ± 6	7 ± 2	14 ± 11	107 ± 63

*Majority of this category is *Calanus finmarchicus*.
**Majority of this category is copepodite stages I-III of *Centropages, Paracalanus, Pseudocalanus,* and *Clausocalanus*.

Table 8. Zooplankton species composition and average concentration (individuals m^{-3}) ± SE per net during Cycle 2. Not all Nets of the same number sampled the same depth in the water column: Net 1 represents the deepest depth bin of the MutliNet, and Net 5 represents the shallowest depth bin (n=6 per net).

	Net 1 (~144-175m)	**Net 2** (~107-143m)	**Net 3** (~71-106m)	**Net 4** (~35-72m)	**Net 5** (~0-34m)
*Calanus spp.**	156 ± 32	203 ± 33	275 ± 61	55 ± 13	36 ± 7
Centropages spp.	18 ± 11	1 ± 1	9 ± 5	96 ± 90	1901 ± 1045
Copepoda**	32 ± 21	13 ± 11	10 ± 9	46 ± 39	1728 ± 1081
Metridia spp.	58 ± 18	44 ± 12	31 ± 7	49 ± 32	40 ± 31
Microcalanus spp.	59 ± 23	88 ± 37	82 ± 26	29 ± 20	5 ± 8
Oithona spp.	75 ± 16	52 ± 15	25 ± 4	176 ± 94	393 ± 116
Paracalanus spp.	2 ± 2	1 ± 2	2 ± 2	17 ± 13	258 ± 145
Pseudocalanus spp.	9 ± 6	6 ± 5	8 ± 4	13 ± 5	61 ± 49

*Majority of this category is *Calanus finmarchicus*.
**Majority of this category is copepodite stages I-III of *Centropages, Paracalanus, Pseudocalanus,* and *Clausocalanus*.

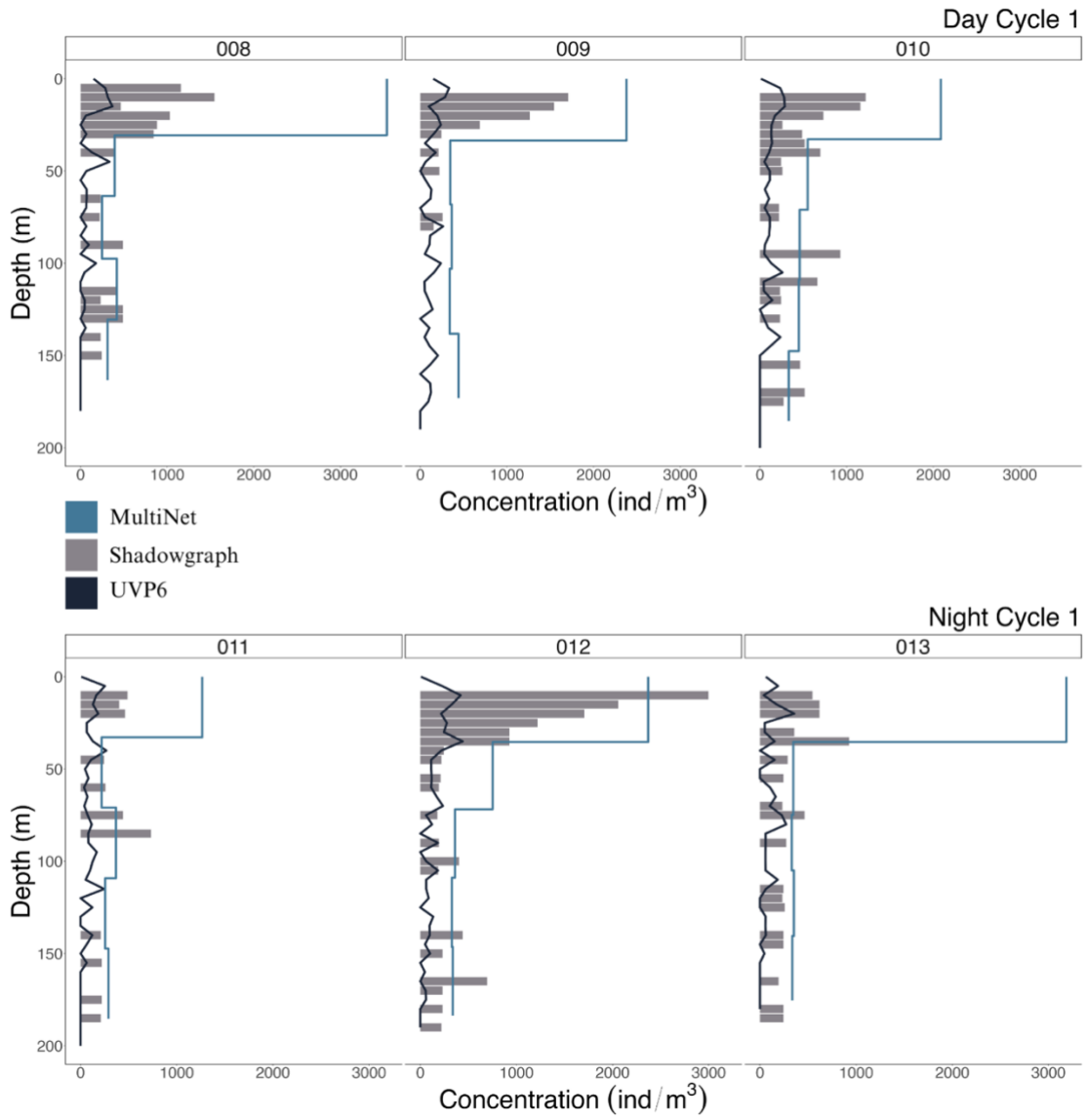

Figure 12. Vertical variation in total copepod concentration (individuals m^{-3}) throughout the water column at each station in day and night for Cycle 1. The blue line represents concentrations estimated using the MultiNet in five depth strata of the water column, the grey bars are concentrations estimated in 5-metre bins using the shadowgraph camera, and the black line is the concentration estimated in 5-metre bins using the UVP6. Station number (008 to 013) is shown at the top of each subpanel.

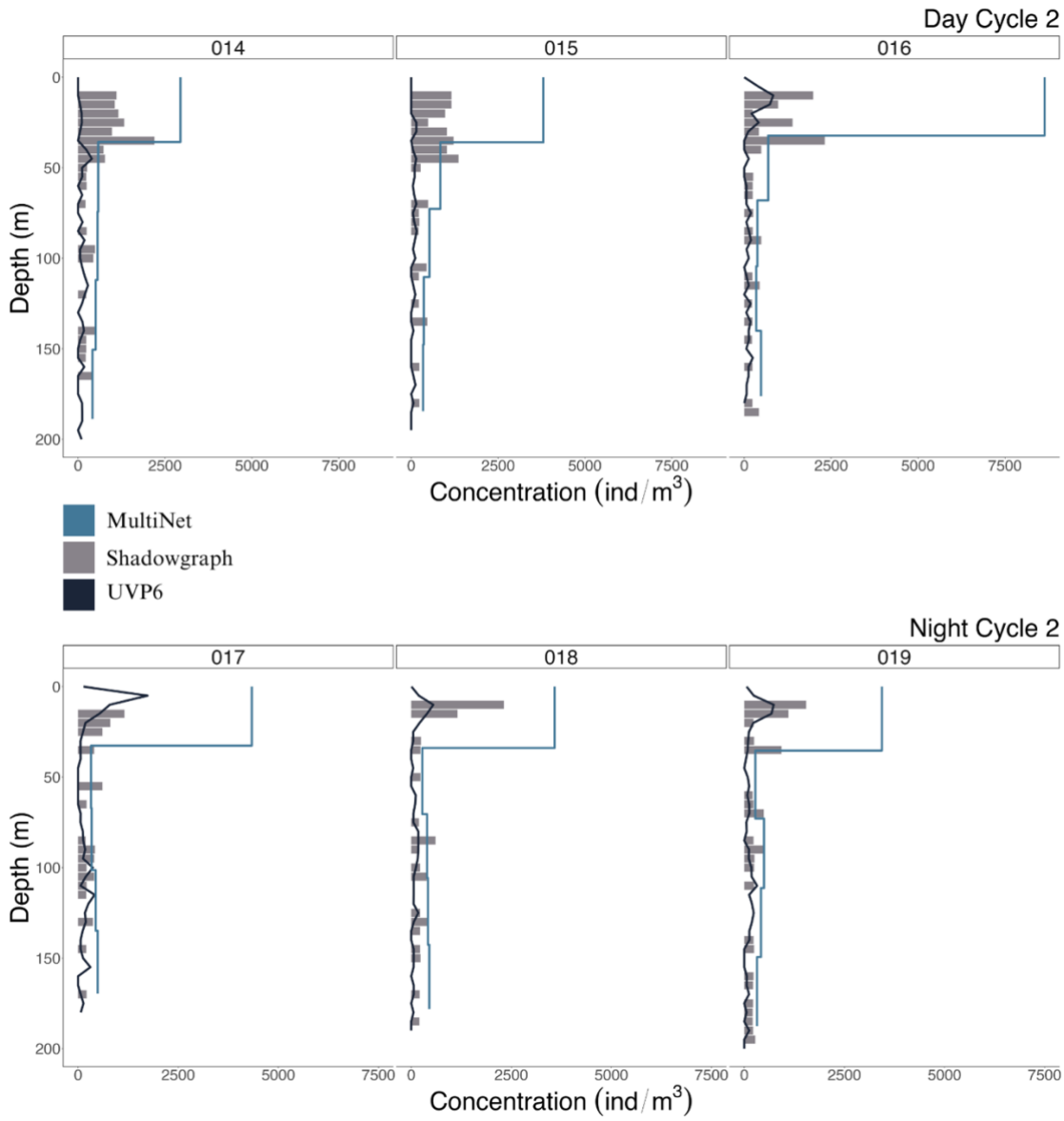

Figure 13. Vertical variation in total copepod concentration (individuals m^{-3}) throughout the water column at each station in day and night for Cycle 2. The blue line represents concentrations estimated using the MultiNet in five depth strata of the water column, the grey bars are concentrations estimated in 5-metre bins using the shadowgraph camera, and the black line is concentrations estimated in 5-metre bins using the UVP6. Station number (014 to 019) is shown at the top of each subpanel.

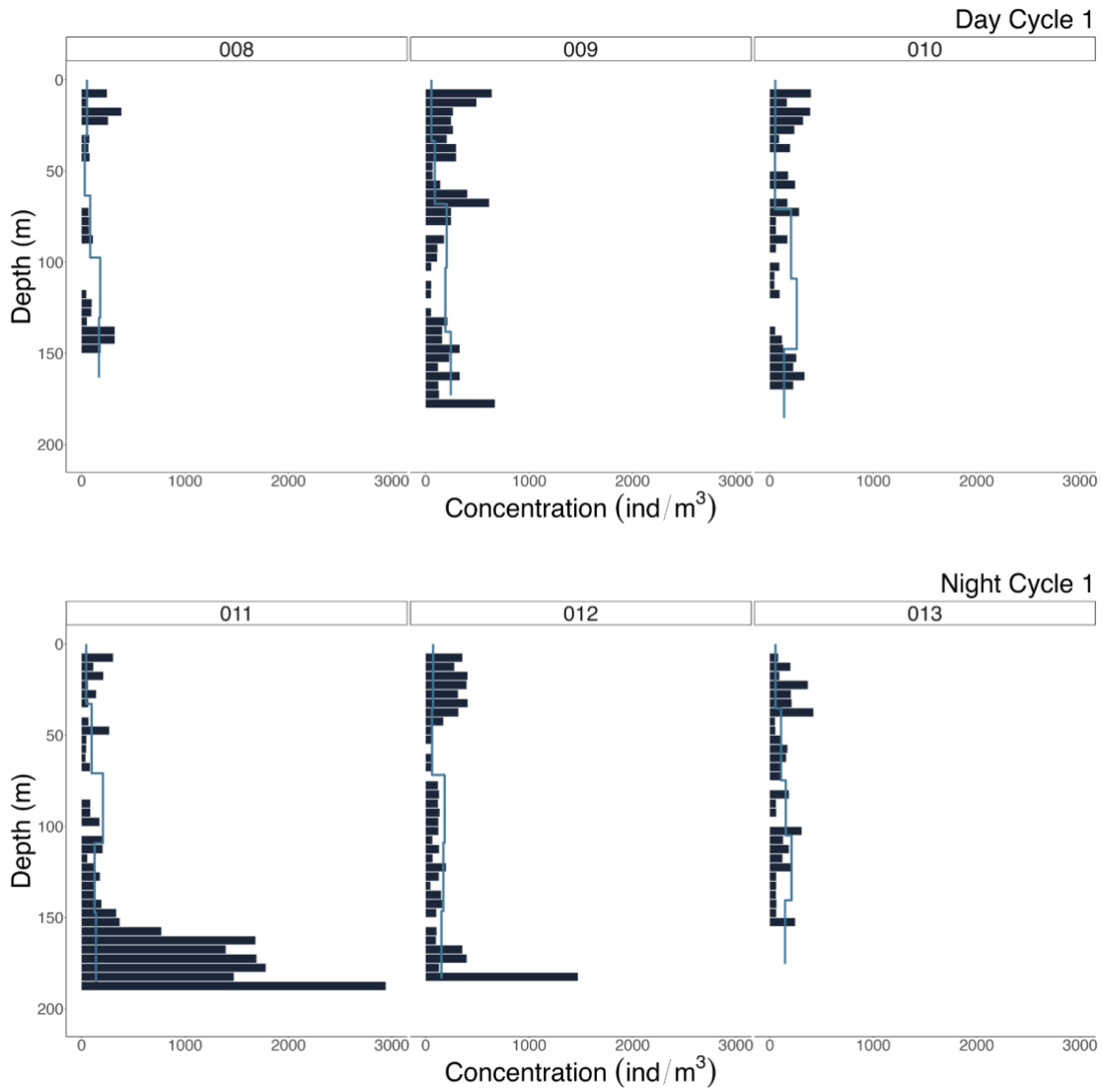

Figure 14. *Calanus finmarchicus* concentration (individuals m^{-3}) measured by the MultiNet (blue line) and 1.6 – 2mm equivalent spherical diameter particles (black bars) (# m^{-3}) measured by the UVP6 throughout the water column in day and night for Cycle 1. Station number (008 to 013) is shown at the top of each subpanel.

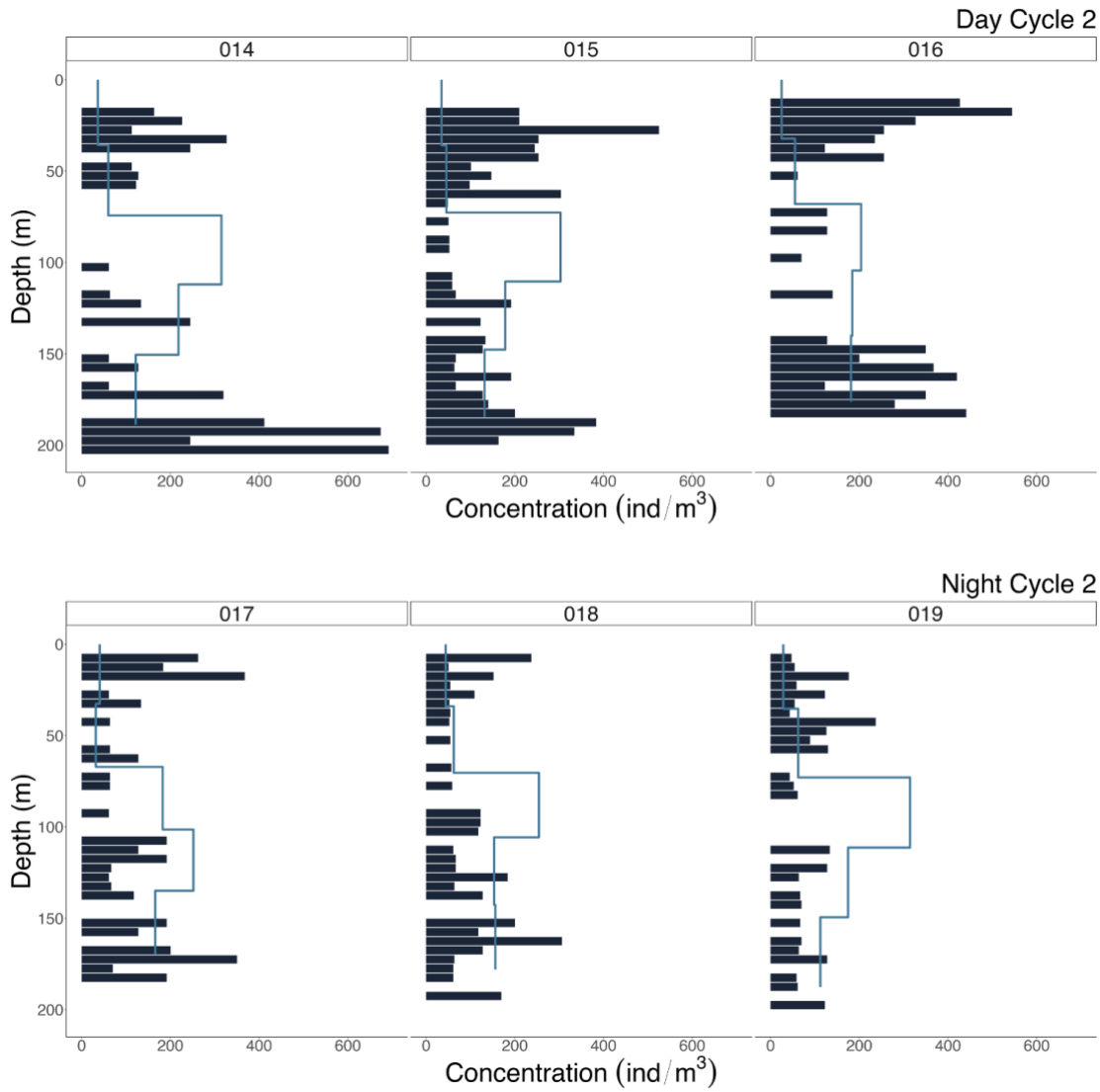

Figure 15. *Calanus finmarchicus* concentration (individuals m^{-3}) measured by the MultiNet (blue line) and 1.6 – 2mm equivalent spherical diameter particles (black bars) (# m^{-3}) measured by the UVP6 throughout the water column in day and night for Cycle 2 derived from MultiNet data. Station number (014 to 019) is shown at the top of each subpanel.

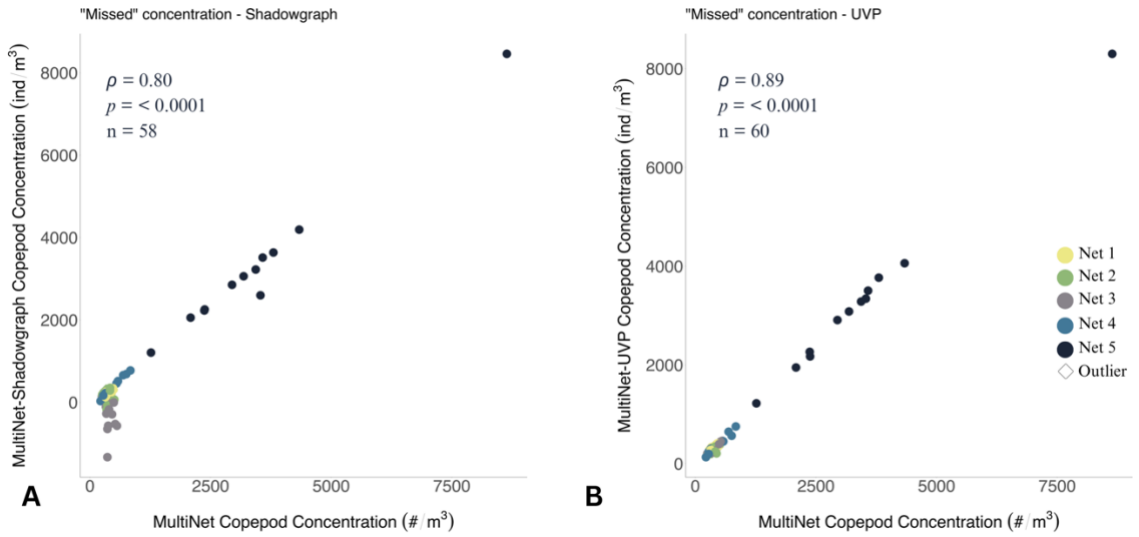

Figure 16. Effect of masking of copepods by other copepods. Scatter plots show the relationship between copepod concentration in the water column measured by the MultiNet (# m^{-3}) and the difference in copepod concentration between the MultiNet and either imaging sensor A) shadowgraph and B) UVP6.

Inter-instrument correlations of copepod concentration varied but were significant across all comparisons (Figure 17). All correlations across the five net depths were significant both when using definite identifications only and when using the sum of definite and possible identifications ($p < 0.05$) (Figure 17). The smallest correlation coefficient (0.30) was found between C_{uvp} and C_{shadow} when using definite-only identifications. The highest correlation coefficient (0.73) was found when comparing C_{net} and C_{shadow} using definite-only identifications and decreased slightly when including possible identifications. Conversely, when comparing C_{net} and $C_{uvp,}$ the correlation coefficient increased substantially when including possible identifications. The same was found when comparing C_{shadow} and C_{uvp}.

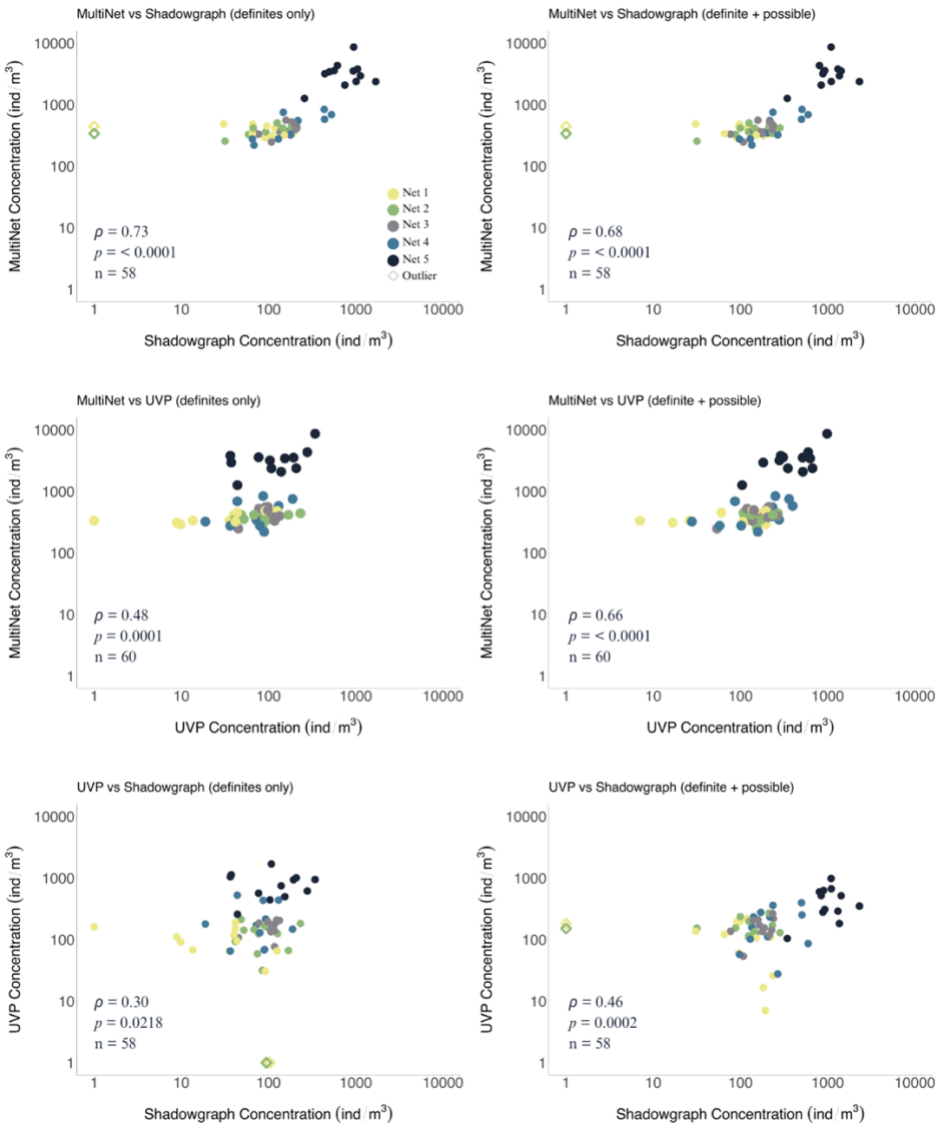

Figure 17. Scatter plots of C_{net} (copepod concentration from the MultiNet) correlated with A) C_{shadow} (copepod concentration from the shadowgraph) using definite identifications only and B) C_{shadow} using the sum of definite and possible identifications, C) C_{uvp} (copepod concentration from the UVP) using definite identifications only and D) C_{uvp} using the sum of definite and possible identifications, C_{uvp} correlated with E) C_{shadow} using definite identifications only and F) C_{shadow} using the sum of definite and possible identifications. Net 1 is shown in yellow, net 2 in green, net 3 in grey, net 4 in blue, and net 5 in black. Statistical outliers are indicated by a diamond shape.

3.2 INFLUENCE OF MARINE SNOW ON DETECTABILITY OF COPEPODS IN IMAGERY

Fluorescence and marine snow concentration were used to determine if bloom conditions were occurring in the water column. Fluorescence was higher later in the month of September, and the highest concentrations of fluorescence did not overlap with the highest concentrations of marine snow in the water column. The early-month stations showed average maximum fluorescence of 3.2 $\pm$ 0.5 mg m^{-3}, and the late-month stations showed maximum averaged fluorescence of 6.5 $\pm$ 0.9 mg m^{-3} (Figure 18). The marine snow showed a maximum averaged concentration at Cycle 1 of 80,700 $\pm$ 102,000 particles m^{-3} and a maximum at Cycle 2 of 64,000 $\pm$ 20,000 particles m^{-3}. Fluorescence values peaked in the top 50 metres of the water column, whereas marine snow particles were highest in concentration at depth, at around 150 metres depth and below. The deep layer of high marine snow abundance was very thick (~50 metres in each cycle). This is the inverse of what is seen in the copepod data, meaning the highest concentrations of copepods and marine snow do not overlap. However, given that marine snow concentrations are overall several times larger than copepod concentrations, the concentrations of marine snow particles in the upper layers of the water column are comparable to those of the copepods.

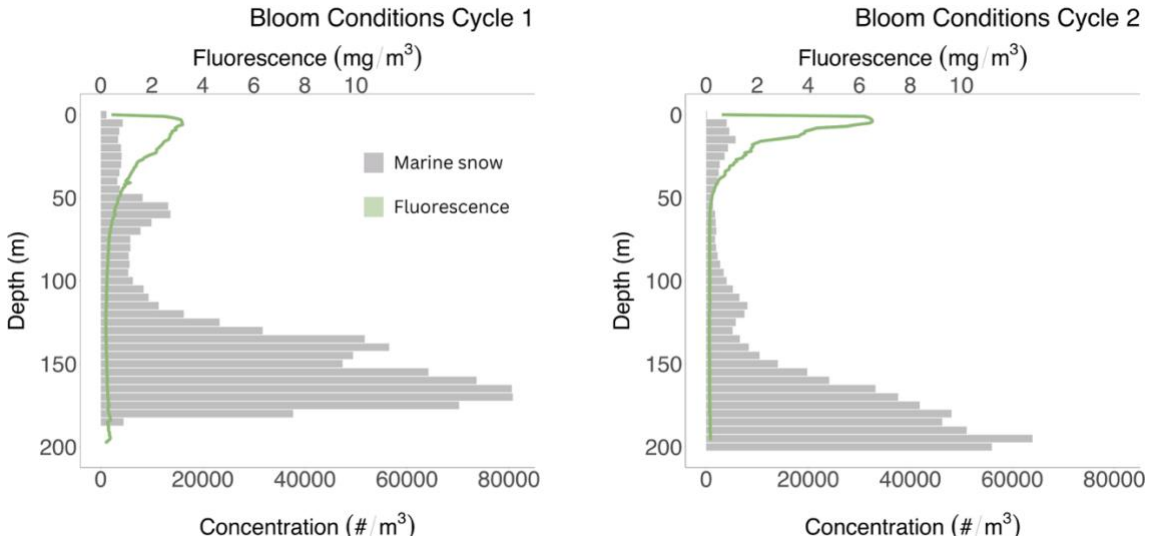

Figure 18. Bloom conditions during Cycle 1 (early September) and Cycle 2 (late September) in the Bay of Fundy. Concentration of marine snow particles are shown as grey bars in # m^{-3} and fluorescence values are shown as green lines in mg m^{-3}.

Since a difference in average maximum marine snow concentration was detected between shallow and deep depths in the water column, I tested whether increased marine snow concentration affected the ability to assign a definite identification to copepod ROIs. The highest ratio of definite to possible identifications was seen in the MultiNet samples (as all microscope identifications are always definite at the taxonomic level of "Copepoda"), followed by the shadowgraph and then the UVP6. The ratio of definite to possible identifications was lowest in the UVP6 imagery with 59% of all annotations falling under the possible category (Figure 19). Figures 20 and 21 show the trend of high possible identifications throughout the water column as detected by the UVP6. However, this ratio of identifications was not significantly affected by increased marine snow concentration (Wilcoxon, $p = 0.88$, n = 60) (Spearman, $\rho = -0.04$, $p = 0.73$, n = 60) (Figure 22).

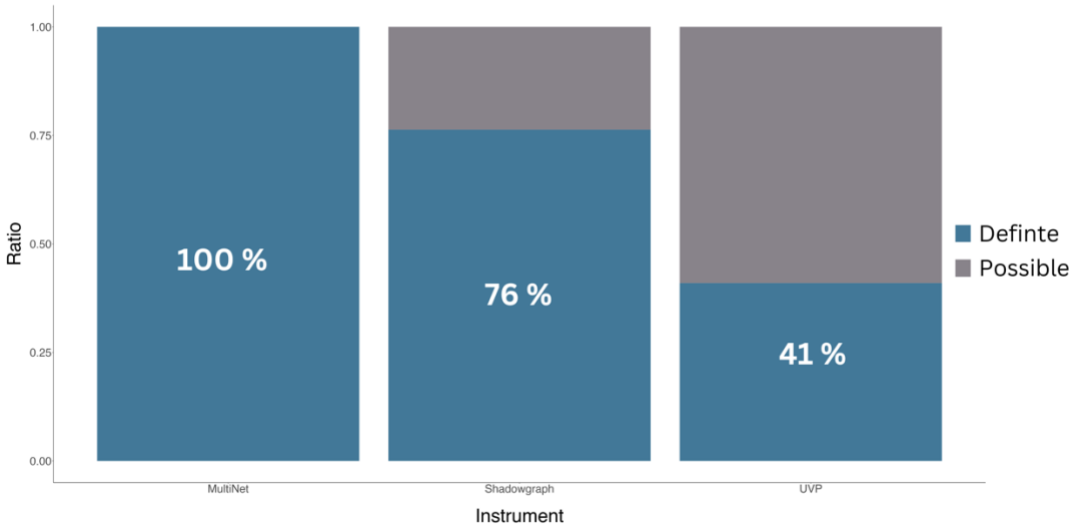

Figure 19. The ratio of definite and possible copepod identifications as measured by the MultiNet, shadowgraph camera, and UVP6 at all stations and depth strata. Blue shows the proportion of definite identifications and grey shows the proportion of possible identifications.

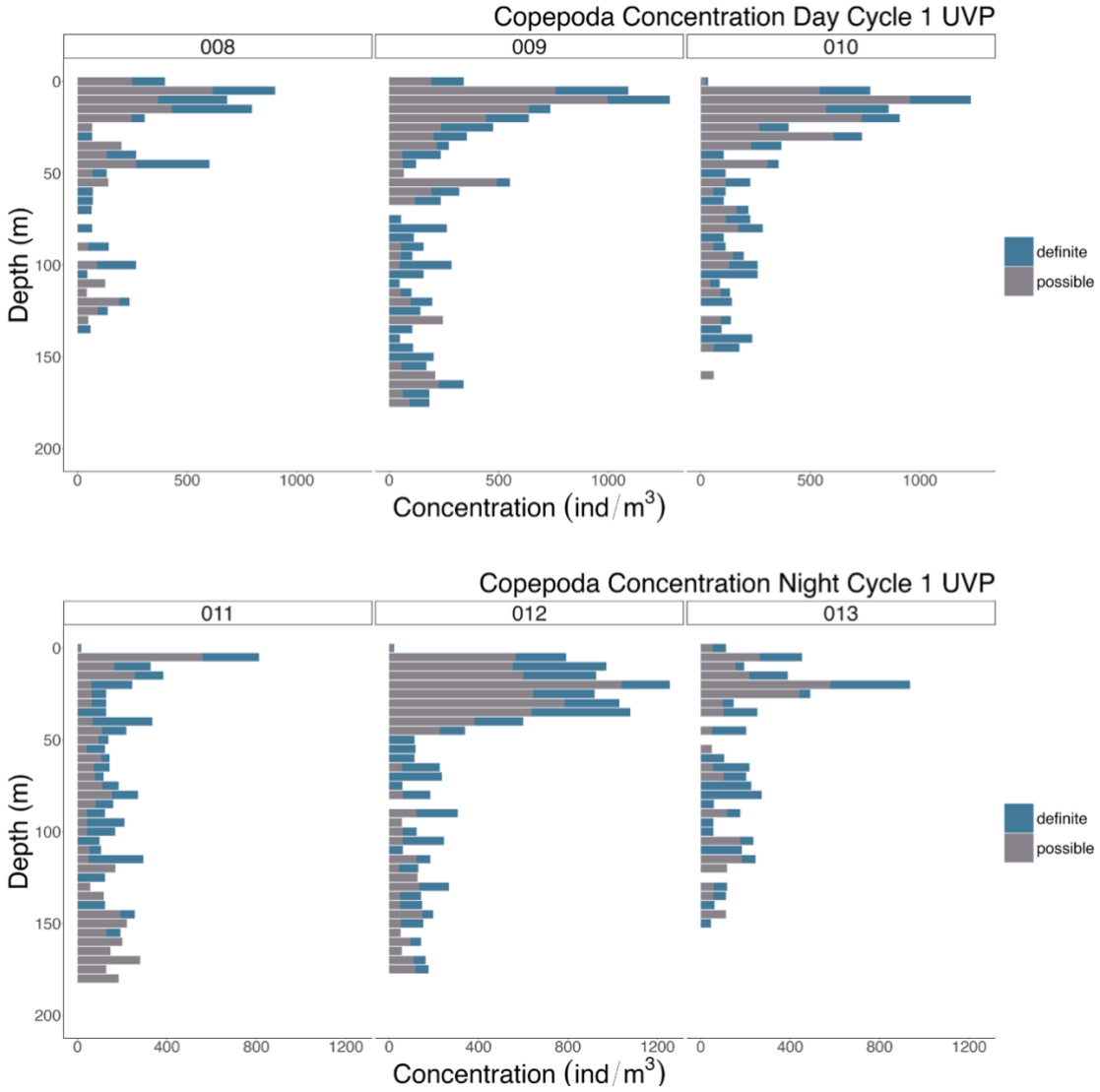

Figure 20. Ratio of definite to possible copepods in UVP6 imagery shown as concentration of copepods in individuals m^{-3} throughout the water column during Cycle 2. Blue shows the proportion of definite identifications and grey shows the proportion of possible identifications.

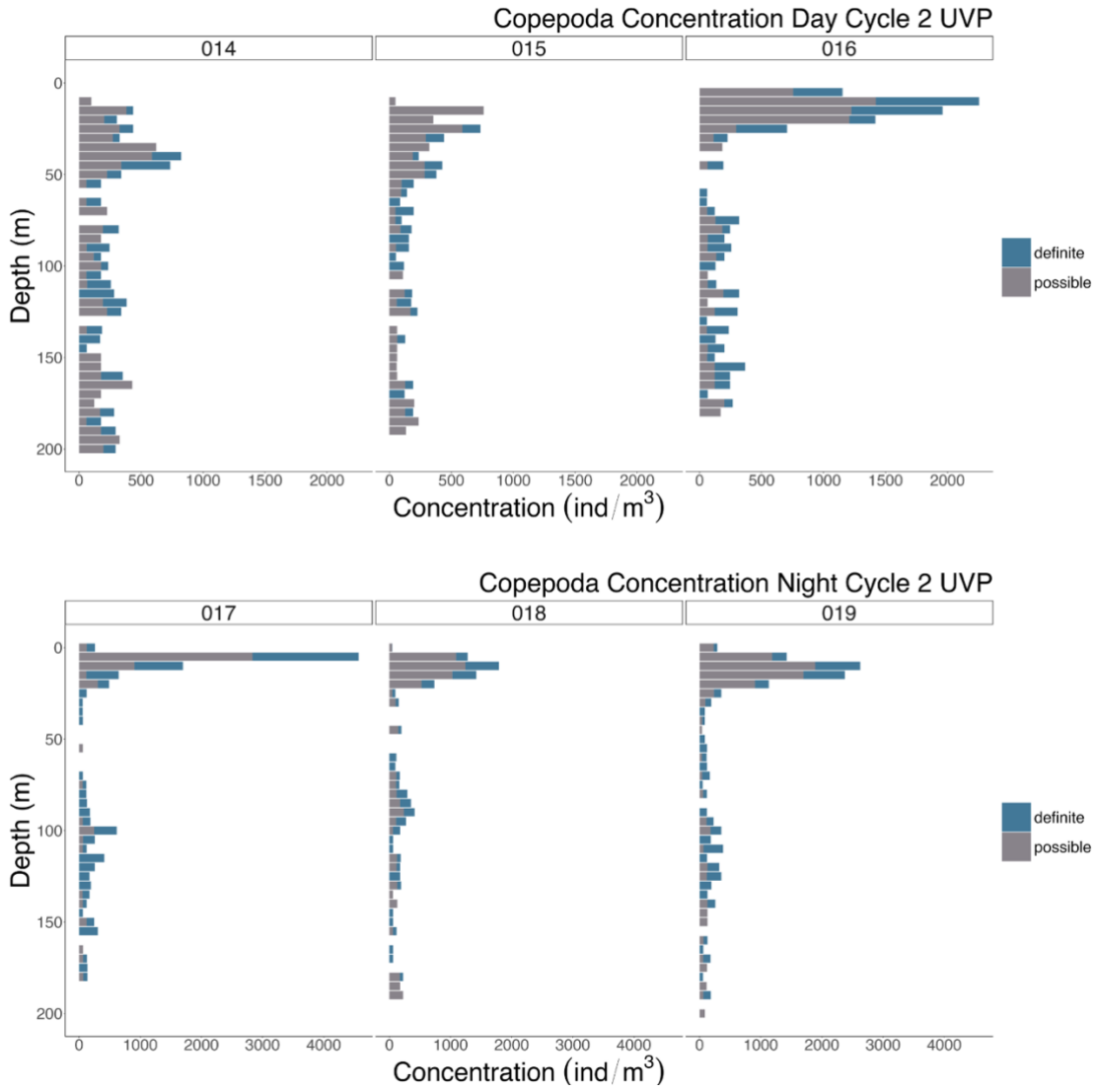

Figure 21. Ratio of definite to possible copepods in UVP6 imagery shown as concentration of copepods in individuals m^{-3} throughout the water column during Cycle 2. Blue shows the proportion of definite identifications and grey shows the proportion of possible identifications.

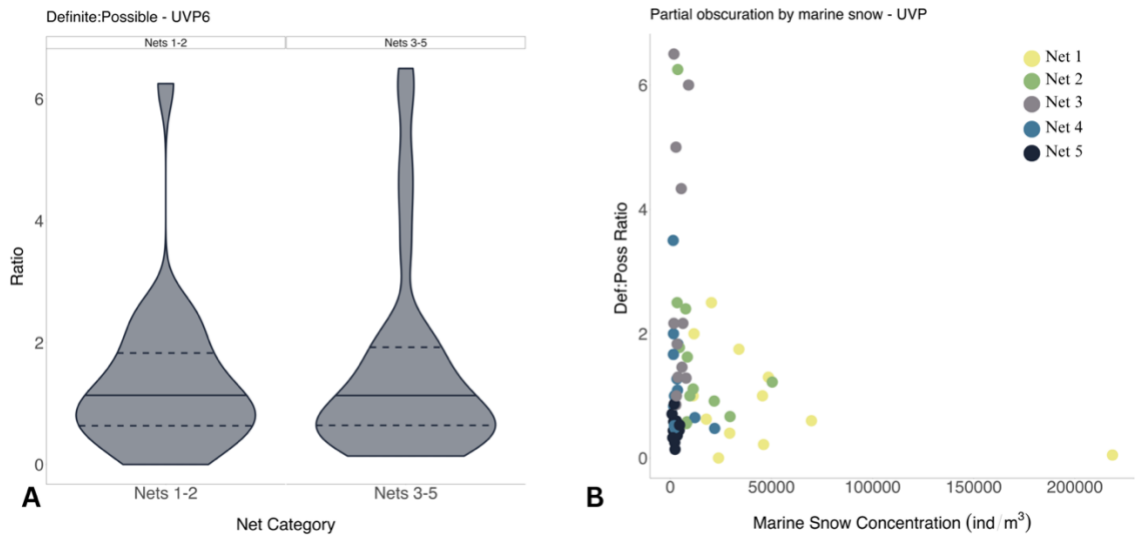

Figure 22. Effect of partial masking of ROIs by marine snow in UVP imagery. A) violin plot of the Definite:Possible identification ratio of copepods in Nets 1 – 2 (higher concentration of marine snow) and Nets 3 – 5 (lower concentration of marine snow) as measured by the UVP6. The solid black line indicates the median and the dashed black lines indicate the upper and lower quantiles. B) scatter plot of marine snow concentration (ind m^{-3}) versus the Definite:Possible identification ratio of copepods throughout the five MultiNet nets.

The ratio of possible to definite identifications in the shadowgraph imagery favoured the definites at 76% (Figure 18). Figures 23 and 24 depict the predominance of definite identifications throughout the water column during both cycles, again in contradiction to my hypothesis that definite identifications would be more difficult under high marine snow concentration conditions (Wilcoxon, *p=0.29,* n=37) (Spearman, ρ = 0, *p* = 0.98) (Figure 25).

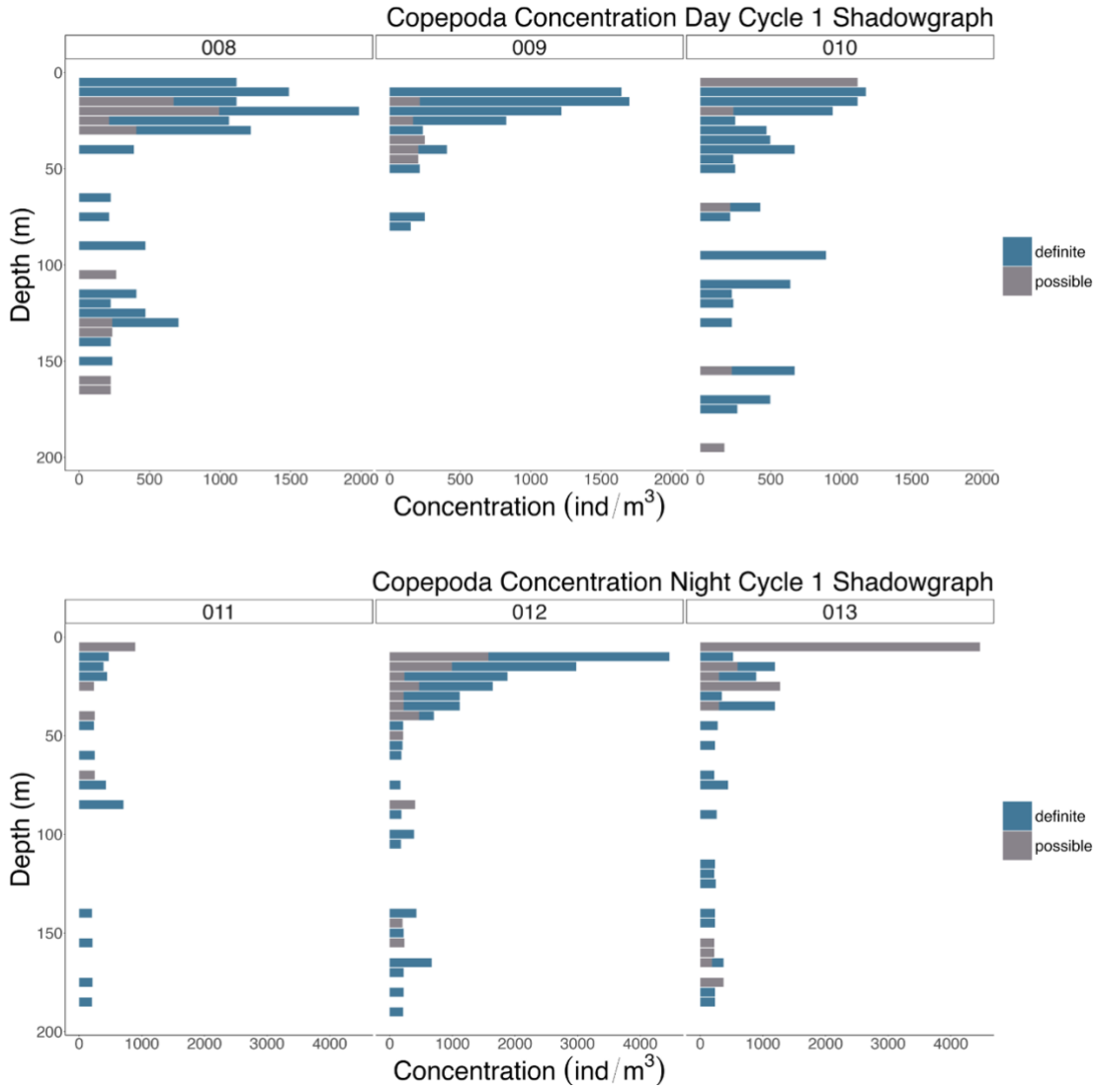

Figure 23. Ratio of definite to possible copepods in shadowgraph imagery shown as concentration of copepods in individuals m^{-3} throughout the water column during Cycle 1. Blue shows the proportion of definite identifications and grey shows the proportion of possible identifications.

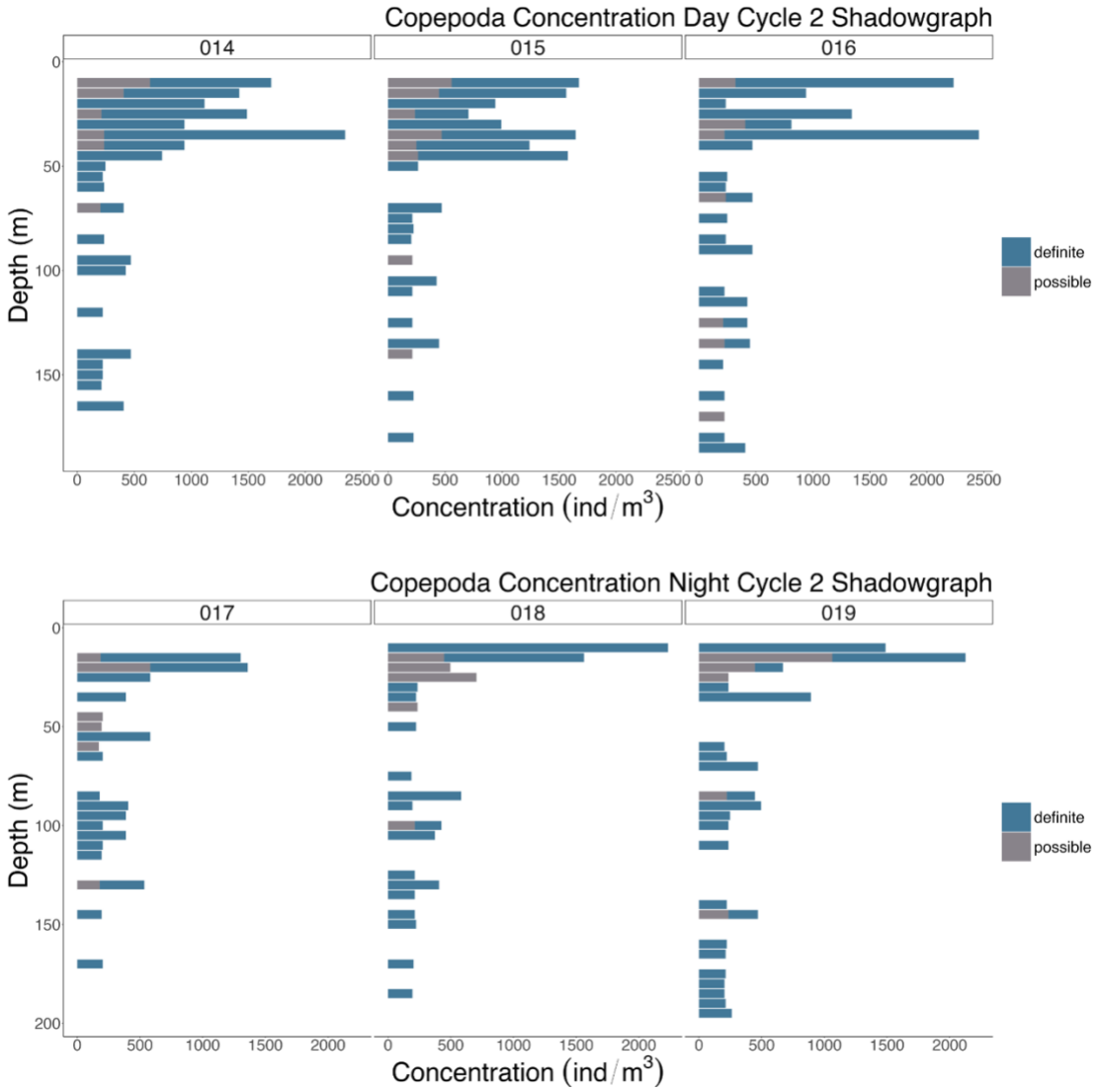

Figure 24. Ratio of definite to possible copepods in shadowgraph imagery shown as concentration of copepods in individuals m^{-3} throughout the water column during Cycle 2. Blue shows the proportion of definite identifications and grey shows the proportion of possible identifications.

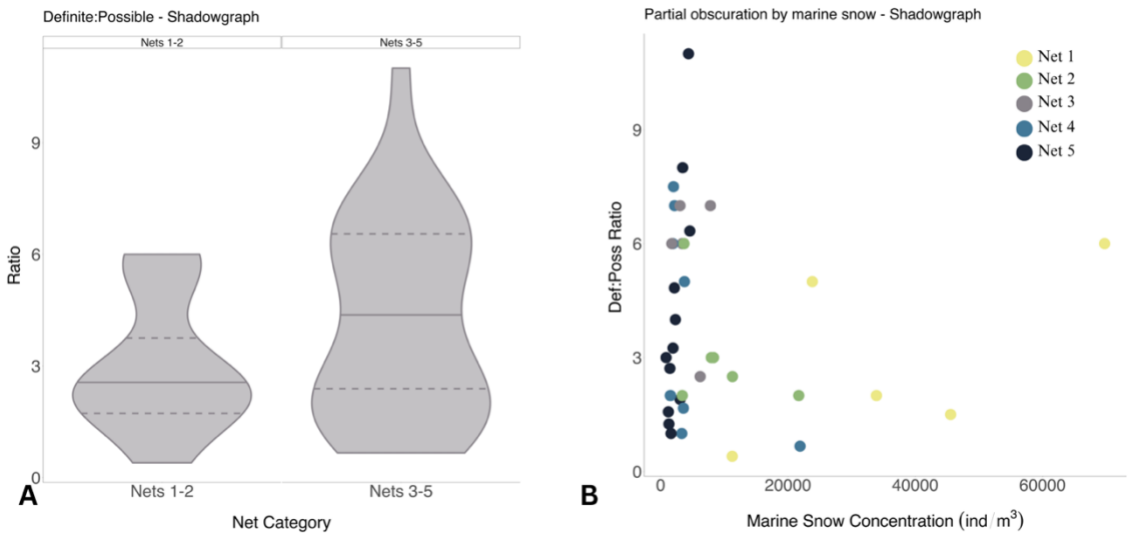

Figure 25. Effect of partial masking of ROIs by marine snow in shadowgraph imagery. A) violin plot of the Definite:Possible identification ratio of copepods in Nets 1 – 2 (higher concentration of marine snow) and Nets 3 – 5 (lower concentration of marine snow) as measured by the shadowgraph. The solid black line indicates the median and the dashed black lines indicate the upper and lower quantiles. B) scatter plot of marine snow concentration (ind m^{-3}) versus the Definite:Possible identification ratio of copepods throughout the five MultiNet nets.

It was thought that heavy marine snow in the water column could decrease the detectability of ROIs in the imagery. Both instruments showed an inverse relationship between marine snow concentration and the absolute concentration of copepods "missed" by either sensor, with the relationship being significant for the UVP6 (Figure 26).

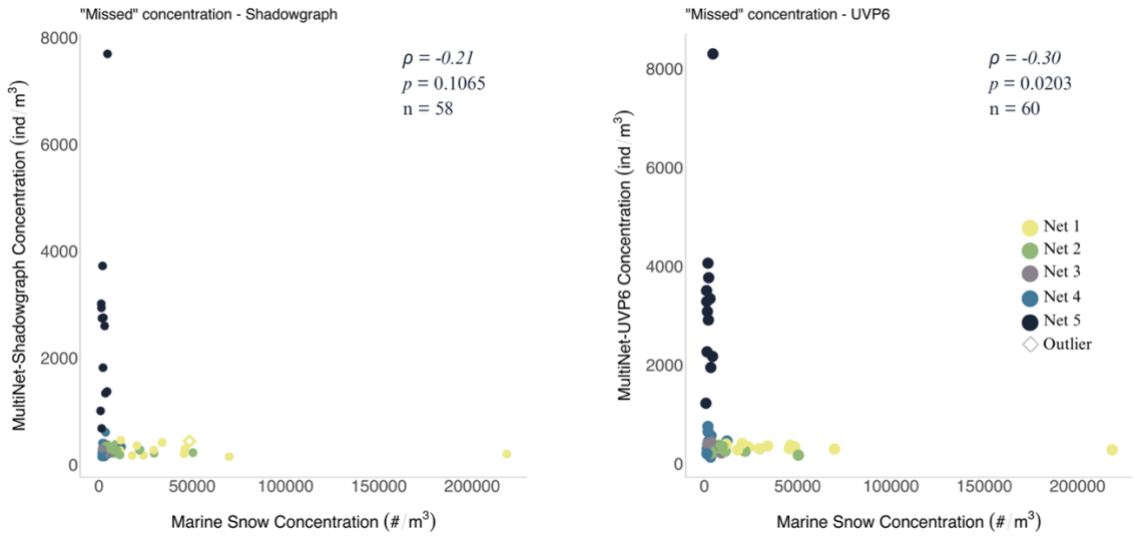

Figure 26. The relationship between marine snow concentration in the water column (# m^{-3}) and the difference in concentration between the MultiNet and either imaging sensor A) shadowgraph and B) UVP6.

3.3 NET AND DAY/NIGHT EFFECT ON COPEPOD VERTICAL LAYERS

There was no significant interaction between net (i.e depth) and day/night on the copepod concentration in any of our instruments nor on the *Calanus* concentrations from the MultiNet. However, a significant main effect of the net was observed on the $\log_{10}$-transformed concentration of copepods in all three instruments (Two-way ANOVA, Tables 9-12, Appendix D) (Figure 26). A significant effect of net was also found on *Calanus* concentrations from the MultiNet. Only definite identifications were used from the imagery data.

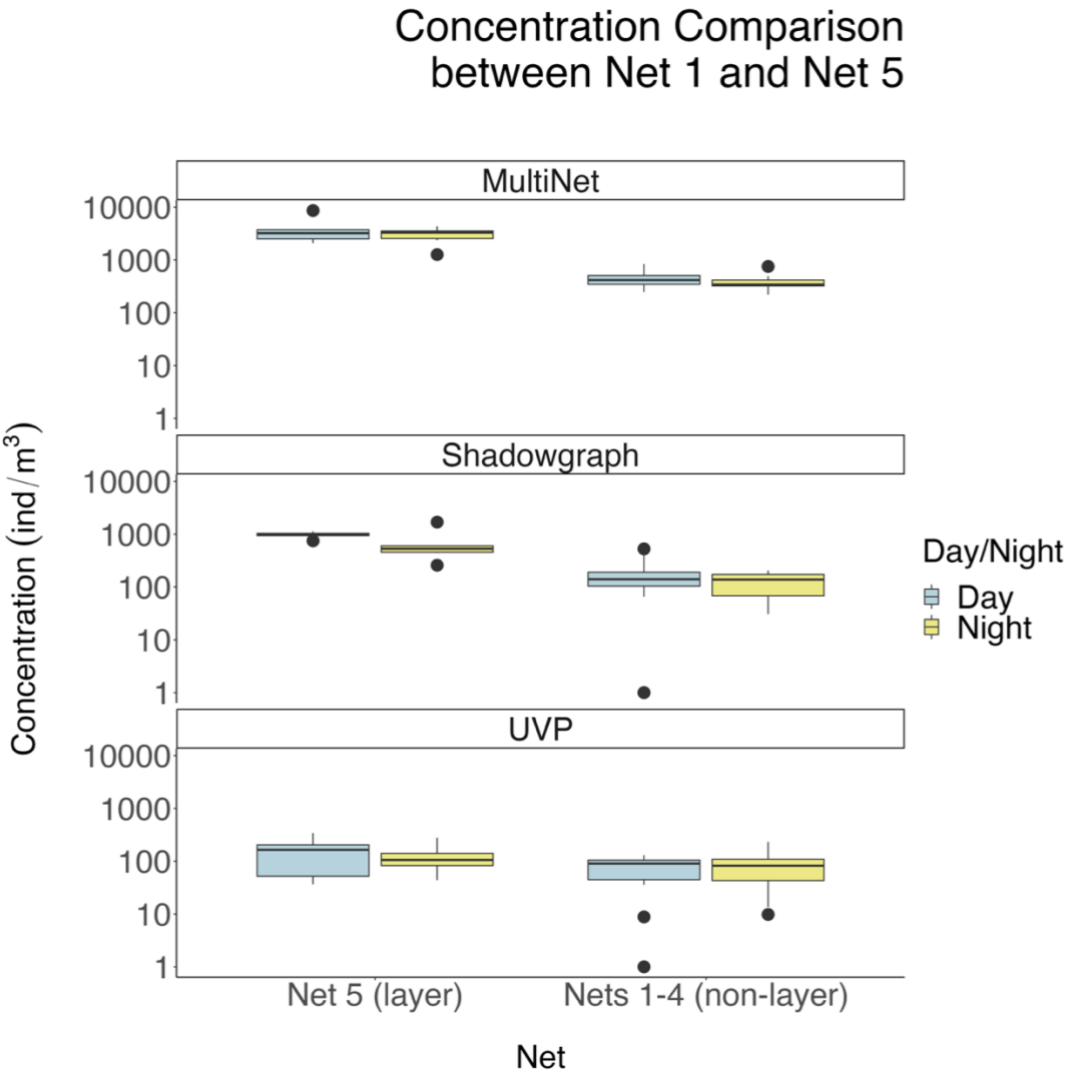

Figure 27. Log_{10}-transformed copepod concentrations (in # individuals m^{-3}) between non-layer depths (nets 1-4) and layer depths (net 5) as measured by the MultiNet, shadowgraph camera, and UVP6. Blue indicates day stations and yellow indicates night stations.

4. DISCUSSION

In this study, I tested the performance of a novel shadowgraph camera for measuring key characteristics of zooplankton *in situ*. The characteristics I was most interested in were vertical distribution, concentration, detection of thin layers, and taxonomic information about the community. These are common population and community characteristics required to better understand plankton ecology and assess the ecosystem state for various management questions/concerns..

4.1 TAXONOMIC IDENTIFICATION

The taxonomic resolution of animals derived from manual visual inspection differed among the three sampling instruments. Visual expert examination of MultiNet samples was able to achieve genus or species level identifications, but taxonomic resolution for the shadowgraph and UVP6 was limited, and definite identification beyond family was rare. Visual inspection of the images showed that the relatively higher image resolution of the shadowgraph to be an advantage over the images from the UVP6. This increased resolution that may have helped achieve finer identifications using imagery from this instrument.

The majority of animals identified in images from the three instruments belonged to Copepoda. This is similar to what other net and sensor comparison studies have found, and reflects the high abundance of copepods in the water column (Benfield et al., 1996; Forest et al., 2012). While identification to genus was rare in images, the UVP6 imagery

could be used to occasionally identify two copepod genera (*Calanus* and *Paraeuchaeta*), while the shadowgraph imagery was able to be used to occasionally identify four genera (*Calanus, Paraeuchaeta, Centropages*, and *Oithona*). This precision level of taxonomic detail in the shadowgraph is comparable to what has been found in other glider-mounted shadowgraph studies with some key differences. Whitmore et al. (2019) used their *Zooglider* system to generate vertical concentration profiles for the genus *Oithona* (which was not achievable in the present study), with all other observed copepods being reported as "Other Copepoda". *Zooglider* can distinguish three different species of *Oithona* from one another in the imagery, and occasionally identify other copepod genera (Ohman, 2019). Identifications made in both of these studies were done after applying a double-pass of a Canny Edge Detector that enhanced the edges of the ROIs. It is possible that a similar method applied to the images collected in this study could increase the visibility of identifying features in the copepods and therefore the frequency at which they can be identified to genus, enabling the generation of concentration profiles for specific genera throughout the water column.

There were some diagnostic features that allowed occasional identification of some copepod genera. *Calanus* is an abundant copepod with some features in the imagery that aided visual identification such as the presence of an oil sac and relatively large body size. *Paraeuchaeta* is a large, though relatively rare, copepod with distinct mandibles that are used to manipulate prey. Mandibles, large body size, and an enlarged genital pore in females, can be used to distinguish it from other copepods. Given that this copepod was rare in the MultiNet samples, it was impressive that the imagers, which sample a much smaller volume of water, captured it at all. The large size of both of these copepods meant that these identifying features did not necessarily need to rely on high image resolution to

be detected. *Centropages* and *Oithona* are two small copepod genera that were identified based on the presence of metasome points and egg sac shape, respectively. Given the small size of these copepods, image resolution is important for picking up on these minute identifying features. In some cases, identification of these genera was possible with the shadowgraph imagery, but not the UVP6 imagery. As with all identifications in the imagery, taxonomic categorization of increasingly finer detail depended heavily on the orientation of the animal relative to the camera. Detection of identifying features like metasome points, genital pores, and especially size, can all be distorted or hidden as the position of the copepod relative to the camera begins to veer from parallel. It is for these reasons that copepods could often not be identified more finely.

Confidence in the copepod identifications made using the three instruments varied. Assessing animals under a microscope always led to a definite identification of copepods that were present in the net. In imagery, however, ROIs can be more ambiguous to the naked eye. The inability to manipulate an image to look at identifying features of an animal in various orientations and lighting conditions can limit the taxonomic identification by conventional means. This is true for the precision of the identification (e.g. to family rather than genus) and for the confidence in the precision of the identification. This can lead to some ROIs being assigned an identification of "possible". This is a key area where machine learning systems may aid identifications when libraries of known species from various orientations are compiled.

The difference in possible versus definite detections of copepods between the two imagers could be due to image resolution. While both imaging devices suffered from the inability of an analyst to manipulate the images to gain the highest taxonomic precision, the shadowgraph camera produced ROIs with more defined edges around the boundary of

each animal's body, which provided an advantage particularly when classifying small organisms. Although, there is a limit to this, as demonstrated by Whitmore et al. (2019) when they found difficulties assigning definite identifications to nauplii in their imagery. Nonetheless, clear boundaries of an animal's body in imagery helps with trait identification (in the case of Copepoda, identifying traits can include antennae, legs, the urosome, and body shape) that can lead to higher confidence in a taxonomic identification. The UVP6 produced high-quality images of relatively large ROIs (see Figure 6 for examples), but the shadowgraph was able to maintain defined edges of ROIs even as they diminished in size, enabling higher taxonomic certainty across a wider range of sizes.

Salps and siphonophore larvae (siphonulae) were regularly imaged by the shadowgraph camera usually above 100 metres depth. Salps are commonly found in plankton nets, but siphonulae are not. Benfield et al. (2003) found these larvae in VPR imagery in the Gulf of Maine at varying depths, although in considerably lower concentrations (a maximum of 96.6 individuals m^{-3}, while our shadowgraph camera recorded a maximum of 491 individuals m^{-3}). While siphonophores have been found in MultiNet samples in the Bay of Fundy over the 2020-2022 sampling seasons, the larval life stage of this taxa (siphonulae) was not captured in our net samples. It is thought that siphonulae appear less frequently in net samples due to their small size and delicate morphology, but that they are important acoustic scatterers in the ocean because they have a gas-filled pneumatophore that scatters sound extremely well. Enumerating their abundance is important for hydroacoustic studies of zooplankton because of their strong acoustic backscatter relative to their biomass (Benfield et al., 2003). Siphonophores, in general, serve as a prey item for turtle, bird, and invertebrate species (Hetherington et al., 2022), so the importance of monitoring their populations should be highlighted. The

shadowgraph camera has shown promise to be an effective tool for capturing siphonulae and should be explored further for this application.

4.2 COPEPOD VERTICAL DISTRIBUTION AND CONCENTRATION ESTIMATES

Copepod concentrations were significantly higher in the top layer of the water column as measured across all three instruments. This layer was comprised of high abundances of small copepods like *Centropages spp., Oithona spp.* and early copepodite stages of *Centropages, Paracalanus, Pseudocalanus and Clausocalanus* who are known to be most abundant in the upper layers of the water column, even during the day (Head et al., 2022; Lewis and Sameoto, 1988; Turner and Dagg, 1983). Because these small copepods do not always exhibit diel-vertical migration, this layer persisted across all stations, resulting in the lack of a significant interaction between net number (i.e. depth bin in the water column) and whether the sample was collected during the day or at night. *Calanus* was more abundant in mid-water during both day and night, indicating that the animals were in diapause, which is their normal physiological state in September (Baumgartner, 2003). *Calanus* abundances were low overall, but particularly so in comparison to non-*Calanus* particles at depth (>150 metres). ROIs belonging to the genus *Calanus* could rarely been identified in the imagery (shadowgraph n = 5; UVP6 n = 2), so variation in concentration of this taxon could not be estimated in the imaging sensor data. Because a diel-vertical migration signal was not detected in the MultiNet samples, it is expected that this signal would not be detected by the imaging sensors either. The agreement between the instruments regarding this is a good indicator that the shadowgraph is able to detect copepod layers in the water column accurately, although it would be

beneficial to confirm this capability by repeating this study in an area where it is expected that the copepod community is undergoing diel-vertical migration.

One of the goals of this study was to be able to quantify *Calanus finmarchicus* concentration in the imagery. Since the imagery was not able to be used to this, I looked at whether size distribution of particles could be used as a proxy. Particle abundance at size in the 1.5 – 2 mm range has been used in the past as a proxy for *Calanus finmarchicus* abundance in Grand Manan Basin in years 1999-2001 (Baumgartner, 2003). However, I found that using UVP6 particles counts within the size range that *Calanus finmarchicus* stage-five is known to occupy as a proxy for *Calanus finmarchicus* concentration may not be suitable at present, because *C. finmarchicus* concentrations are far lower in Grand Manan Basin than in the past and distinct layers of high concentration were not distinguishable from other particle types. UVP6 particles in the 1.6 - 2mm size range and the concentrations of *Calanus finmarchicus* in the MultiNet samples collected in 2022 were not positively correlated. Given that this method of estimating *Calanus finmarchicus* concentration has been used reliably in the past, and the fact that the present study was based on a small sample size, this comparison should be repeated on future cruises and different areas to confirm the findings in the present study.

The correlation between the net and each imaging sensor and identification combination (definite-only or the sum of definite and possible identifications) was significant but varied. The strong, positive correlation between the MultiNet and shadowgraph concentrations using definite-only identifications indicates that the vertical pattern seen throughout the water column was similar in both instruments (although this positive correlation weakened slightly when including possible identifications). A similar overall pattern between shadowgraph imagery and net samples throughout depth was

observed in the *Zooglider* study (Whitmore et al., 2019). Expanding beyond glider-mounted equipment, Sorochan et al. (2023) found a stronger correlation between VPR and JackNet concentration measurements of *Calanus spp.*, although concentrations were vertically-integrated for that analysis. Positive correlations were also found between the MultiNet and the UVP6 in the present study, although the relationship when including possible identifications was stronger than when using definite identifications alone. Correlations between the shadowgraph and UVP6 were the lowest. The highly patchy nature of zooplankton and the inherent differences in how each instrument samples the water column means it is unlikely to see a perfect 1:1 relationship between instruments. However, the fact that all instruments found a significant difference in the concentration of copepods inside versus outside of the layer is a good indicator of the instruments' ability to detect the densest copepod layers in the water column.

Both imaging instruments underestimated copepod concentration. Furthermore, the imaging sensors underestimated the net concentrations more in areas of high copepod density. The result of the correlation test between MultiNet copepod density and "missed" copepod concentration by the imaging sensor would indicate that there is masking of copepods by other copepods, leading to underinflated counts in areas of high density. The tendency for sensors to underestimate concentration in areas of very high density has been seen in a previous sensor versus net study in the same area (Baumgartner, 2003). However, copepods were rarely seen overlapping with each other in the imagery. The densest layer of copepods occurred at the surface, where the community was dominated by small copepods in comparison to deeper layers where larger copepods became more common. It is likely that the detectability of copepods in these corresponding layers had more to do with size than with masking by other copepods.

Initially, it was thought that the discrepancy in absolute concentrations could be attributed to differences in water volume filtered. The MultiNet samples a much larger volume of water in a single cast than is sampled with either imaging sensor. This lower sampling volume is thought to play a factor in lower abundance counts from imagery compared to nets, along with possible avoidance of the sampling equipment by larger zooplankton and/or the inability to detect or resolve the taxonomy of small copepods, which we know in our study to make up the majority of shallow copepod layer (Barth and Stone, 2022; Forest et al., 2012). There is a trade-off between sampling large enough volumes of water for robust concentration estimates while maintaining image resolution that is high enough for taxonomic identification of small animals (Lombard et al., 2019). A previous study found underestimates on the order of 2-5 factors in the concentration of zooplankton when comparing UVPs and nets (Forest et al., 2012). Remsen et al. (2004) found that, even when mounted directly on their net sampler, the Shadowed Image Particle Profiling Evaluation Recorder (SIPPER) still underestimated total copepod abundance, because small, dominant copepods were not well resolved in the imagery. However, the *Zooglider* overestimated the abundances from MOCNESS tows, although there seemed to be good agreement as to the location of layers in the water column (Whitmore et al., 2019). Many small copepods, using the Canny Edge Detector, were detected in the *Zooglider* imagery (sizes that may have not always been clear in our shadowgraph imagery), which had a somewhat higher sampling frequency than the shadowgraph in the present study (2Hz vs 0.8Hz), enabling the *Zooglider* to more accurately sample discrete layers of copepods in the water column than was possible with the equipment in the current study. Sampling frequency abilities have already been augmented in the subsequent iteration of the prototype shadowgraph camera used in this study, but a further study on

the size frequency distributions of the copepods imaged in our study is warranted to determine if small target size contributed to the concentration underestimations. The average factor at which our shadowgraph concentrations deviated from the MultiNet concentrations is on the same scale as reported by the VPR (Benfield et al., 1996). Overall, the shadowgraph camera has demonstrated the ability to detect copepod layers with a reasonable degree of agreement with the net data.

One advantage of using sensors is that they can collect data at finer scales than nets. This can be seen visually in Figures 12 and 13, where the concentration of copepods as measured by the imaging sensors varies within the depth stratum sampled by the MultiNet. While the MultiNet concentration is averaged over 10s of metres, the shadowgraph and UVP6 can collect data at a fraction of a metre, although they are binned here at 5-metre intervals to reduce noise. This feature is extremely useful when zooplankton concentrations vary on the scale of a few metres, as can be the case with *Calanus finmarchicus*. Right whales are thought to target *C. finmarchicus* concentration maxima, sometimes very close to the seafloor (~5 metres) where we cannot sample with nets (Sorochan et al., 2023). Determining where these maxima occur both on the basin scale and vertically in the water column is helpful for discovering suitable habitat, identifying unknown conservation concerns, and explaining patterns observed in planktivore populations.

4.3 IMAGE SENSOR PERFORMANCE UNDER VARYING ENVIRONMENTAL CONDITIONS

Marine snow abundance varies widely in aquatic ecosystems, ranging from <1000 to 53 million aggregates m^{-3}, with higher abundances typically appearing in coastal ecosystems compared to offshore ecosystems (Simon et al., 2002). Marine snow particle concentration can cause difficulty with image processing, particularly when some level of machine learning is being used (Bi et al., 2015; Ohman et al., 2019). Phytoplankton blooms and sediment plumes can lead to higher concentrations of marine snow particles in the water column as the plankton cells turn over and begin to sink to the sea floor (Trudnowska et al., 2021) and could potentially obscure ROIs of zooplankton in the image frame. Because peak phytoplankton blooms occur between spring and fall in the Bay of Fundy (Martin et al., 2009), I tried to plan my study period to sample under bloom and non-bloom conditions, but was not ultimately successful. I found that fluorescence levels were lower during Cycle 1, indicating that the bloom was only beginning, and by Cycle 2, I was sampling mid-bloom. Further, the bloom stage seemed to have little impact on the concentration of marine snow in the water column; it was extremely high in the bottom ~75 m. While fluorescence and marine snow concentration did not correlate as we expected, there was some variation in marine snow particles throughout the water column, so the effect of marine snow concentration on the detectability of copepods could still be examined.

Fortunately, there were no strong indications that the performance of the UVP6 nor the shadowgraph camera at detecting zooplankton suffered under higher marine snow concentrations when manually detecting and classifying ROIs. To understand if this

variation in marine snow particles presented a problem with identifying animals in my imagery, I compared the ratio of definite to possible identifications under different marine snow loads as well as investigated the relationship between marine snow concentration and "missed" copepod concentration. If the number of possible identifications was significantly higher under high marine snow concentrations, or if there was a strong positive relationship between marine snow concentration and "missed" copepod concentration, I would infer some level of obscuring occurred for which future studies would need to accommodate to achieve accurate estimates of zooplankton concentration. While both imaging instruments showed some level of uncertainty in their identifications, this ratio did not change significantly in depth bins where there was a notable increase in marine snow concentration. The negative correlation between "missed" copepod concentration and marine snow concentration is likely due to the coincidental overlap in of the lowest marine snow concentrations with depth bins where copepods were underestimated due to the reasons explored in section 4.2 Future laboratory tests using known concentrations of marine snow and copepods could more precisely quantify the "missed" copepod concentration that is due to masking by marine snow and exclude discrepancies related to zooplankton patchiness.

4.4 SOURCES OF UNCERTAINTY

A source of bias in this study comes from differences in the taxa that each instrument type is known to target or undersample. The UVP6HF is primarily a particle counter, and is designed to target and extract ROIs of particles > 620 μm equivalent

spherical diameter (ESD), where the size of the particle is large enough to distinguish morphological characteristics useful for classification (Picheral et al., 2022). The majority of animals in the thick copepod layer in our study sites were small, with prosomes measuring less than this threshold (Conway, 2006), therefore it is possible that either the ROI was not retained or the animal was too small to be able to reliably use morphometric features to assign a taxonomic identification. On the other hand, the shadowgraph camera could exclude larger, more motile zooplankton that the UVP6 excels at capturing, because of the slow speed that the glider travels at, and that fact that the shadowgraph's imaging system relies on animals flowing through a tunnel. In particular, animals such as euphausiids may be able to sense the glider and avoid the approaching camera sampling tunnel (Guihen et al., 2022). However, another study with very similar equipment to ours found estimates of euphausiids from their camera and net to be similar (Whitmore et al., 2019). Additionally, larger hydrozoans in the present study were observed entangled in the imaging tunnel, leaving only their tentacles in the image frame which precludes taxonomic identification. Larger, mobile plankton are also known to exhibit net avoidance, as they can detect the pressure waves from oncoming nets (Johnson and Allen, 2012), meaning euphausiids also tend to be under sampled by nets. However, under sampling of this taxa can be partially mitigated by fast towing speeds as I have done in this study. One taxonomic group that is famously under sampled by nets are the gelatinous zooplankton. While they may be physically captured, the pressure from towing may break them apart, entangle them in the net, or extrude them from the nets altogether (Remsen et al., 2004). This can lead to post-collection identifications being hindered due to damaged, incomplete, or distorted specimens due to preservation artifacts (Harris et al., 2000; Ohman et al., 2019). In comparison, *in-situ* imagers offer a non-invasive way to image

gelatinous zooplankton in their entirety and provide a reference collection that does not alter with age.

Zooplankton are highly patchy (Folt and Burns, 1999) and as with any multi-instrument comparison where the samplers are not attached to a shared frame or rosette, there can be some uncertainty that the same water mass is being sampled by the different instruments. While the glider is underwater, its exact position is unknown and so concurrent sampling takes careful planning. In this study, we used the glider's last-known position at the surface to align our ship sampling as closely as possible to the glider. Additionally, we sampled with the tides to help ensure that the glider travelled as straight as possible between surfacings, which enabled us higher accuracy in following the intended track line. Finally, we sampled well within the time limits reported by another gear-comparison study (Whitmore et al., 2019b).

4.5 FUTURE DIRECTIONS

This study is the first to use *in-situ* plankton imaging on gliders in Atlantic Canada, and an early example globally. Image identification and annotation in this study was completed manually to create regional image databases for our specific instrumentation. However, manual identification and delinaeation of ROIs in images is arduous but can be augmented, in the future, with the use of machine learning. Machine learning has already proved to be an accurate tool for taxonomic identifications of plankton when using a relatively small number of categories (Gorsky et al., 2010) and other studies, along with the present study, have shown that copepods from wild populations can be identified to genus and species in certain cases (Ohman, 2019) . Recently, machine learning has even

been used to stage copepods from *in-situ* imagery (Maps et al., 2024). However, an automated approach will require a large number of images of each taxa of interest to develop training and test datasets. One way to develop a large library of images of species with known certainty could be by imaging single-stock, live cultures for more precise identifications (i.e. to species), although manual verification of these automatic identifications are likely to be necessary while this technology advances (Giering et al., 2022). The results of the present study have led to image database that is specific to our region and imaging devices, and a next step is to begin to experiment with machine learning to automate the identification portion of this process.

Habitat and prey field monitoring has important conservation applications. North Atlantic right whales (*Eubalaena glacialis*) are among the animals with the highest conservation concerns in Atlantic Canada. Monitoring their prey field for changes in abundance, distribution, and taxonomic composition (especially late-stage *Calanus* spp.) has been, and will continue to be, a key strategy for identifying suitable habitat and explaining patterns we may see in their population. Staging copepods is challenging using techniques other than microscopy, as a key part of their body used for staging (urosome) does not usually appear detailed enough to identify their life stage. However, for *Calanus finmarchicus*, their size frequency distribution per life stage has been extensively studied (Grainger 1963), and stage-five copepodites have been known to be the main occupants of the 1.5 – 2mm equivalent spherical diameter (ESD) range in the zooplankton community (Baumgartner, 2003). In imagery, this known size frequency distribution can be used to stage individuals that have been identified as *Calanus* based on other traits (e.g. body shape). This will help us more precisely identify the maximum concentrations of

Calanus in the water column and determine where we expect North Atlantic right whales to be feeding.

Similar studies to mine have used multiple sensors (imagers and echosounders) on a single glider for monitoring zooplankton and the ocean environment (Ohman et al., 2019; Whitmore et al., 2019). This approach is beneficial not only for inter-instrument comparison but because the use of varied sensors allows the collection of a wider range of data. In addition to sensors used for measuring zooplankton, glider-mounted hydrophones can be used to acoustically detect baleen whale species in near real-time (Baumgartner et al., 2020). An echosounder for measuring zooplankton in real-time has also been studied (Horne et al., 2023). The use of glider-mounted shadowgraph imagery for real-time monitoring will hinge on the development of technology that can analyze the imagery onboard the glider. Systems such as these are power-hungry and could potentially shorten deployments, so a trade-off between image processing power, transfer of verification image subsets, and deployment time will have to be explored. The use of a glider mounted with a hydrophone and a shadowgraph camera would allow concurrent sampling of predator and prey to generate robust datasets of predator habitat use and ecological interactions.

4.6 CONCLUSIONS

The shadowgraph camera has shown to be a useful tool for capturing copepod layers and has promise for being able to refine copepod identifications to the genus level. Future studies in Atlantic Canada can make use of our existing image library to train machine learning models that compound in accuracy over time and can be used to cut

down on the time investment needed to manually validate identifications. Concentration estimates obtained by the shadowgraph underestimated those obtained with the MultiNet, although there was good correlation between the pattern of concentration throughout the water column between two instruments. Inter-instrument comparisons similar to this study can be used in other ocean basins to generate models specific to that area and obtain absolute concentration estimates. Long-term use of the glider-mounted shadowgraph may have the potential to detect spatio-temporal changes in the prey fields of planktivores.

BIBLIOGRAPHY

Álvarez, E., Moyano, M., López-Urrutia, Á., Nogueira, E., Scharek, R., 2014. Routine determination of plankton community composition and size structure: a comparison between FlowCAM and light microscopy. J. Plankton Res. 36, 170–184. https://doi.org/10.1093/plankt/fbt069

Barth, A., Stone, J., 2022. Comparison of an In Situ Imaging Device and Net-Based Method to Study Mesozooplankton Communities in an Oligotrophic System. Front. Mar. Sci. 9, 898057. https://doi.org/10.3389/fmars.2022.898057

Batten, S.D., Clark, R., Flinkman, J., Hays, G., John, E., John, A.W.G., Jonas, T., Lindley, J.A., Stevens, D.P., Walne, A., 2003. CPR sampling: the technical background, materials and methods, consistency and comparability. Prog. Oceanogr. 58, 193–215. https://doi.org/10.1016/j.pocean.2003.08.004

Baumgartner, M., Cole, T., Campbell, R., Teegarden, G., Durbin, E., 2003. Associations between North Atlantic right whales and their prey, Calanus finmarchicus, over diel and tidal time scales. Mar. Ecol. Prog. Ser. 264, 155–166. https://doi.org/10.3354/meps264155

Baumgartner, M.F., 2003. Comparisons of Calanus finmarchicus fifth copepodite abundance estimates from nets and an optical plankton counter. J. Plankton Res. 25, 855–868. https://doi.org/10.1093/plankt/25.7.855

Baumgartner, M.F., Bonnell, J., Corkeron, P.J., Van Parijs, S.M., Hotchkin, C., Hodges, B.A., Bort Thornton, J., Mensi, B.L., Bruner, S.M., 2020. Slocum Gliders Provide Accurate Near Real-Time Estimates of Baleen Whale Presence From Human-Reviewed Passive Acoustic Detection Information. Front. Mar. Sci. 7, 100. https://doi.org/10.3389/fmars.2020.00100

Benfield, M.C., Davis, C.S., Wiebe, P.H., Gallager, S.M., Gregory Lough, R., Copley, N.J., 1996. Video Plankton Recorder estimates of copepod, pteropod and larvacean distributions from a stratified region of Georges Bank with comparative measurements from a MOCNESS sampler. Deep Sea Res. Part II Top. Stud. Oceanogr. 43, 1925–1945. https://doi.org/10.1016/S0967-0645(96)00044-6

Benfield, M.C., Lavery, A.C., Wiebe, P.H., Greene, C.H., Stanton, T.K., Copley, N.J., 2003. Distributions of physonect siphonulae in the Gulf of Maine and their potential as important sources of acoustic scattering. Can. J. Fish. Aquat. Sci. 60, 759–772. https://doi.org/10.1139/f03-065

Benoit-Bird, K.J., Patrick Welch, T., Waluk, C.M., Barth, J.A., Wangen, I., McGill, P., Okuda, C., Hollinger, G.A., Sato, M., McCammon, S., 2018. Equipping an underwater glider with a new echosounder to explore ocean ecosystems: Echosounder equipped glider. Limnol. Oceanogr. Methods 16, 734–749. https://doi.org/10.1002/lom3.10278

Bi, H., Cook, S., Yu, H., Benfield, M.C., Houde, E.D., 2013. Deployment of an imaging system to investigate fine-scale spatial distribution of early life stages of the ctenophore Mnemiopsis leidyi in Chesapeake Bay. J. Plankton Res. 35, 270–280. https://doi.org/10.1093/plankt/fbs094

Bi, H., Guo, Z., Benfield, M.C., Fan, C., Ford, M., Shahrestani, S., Sieracki, J.M., 2015. A Semi-Automated Image Analysis Procedure for In Situ Plankton Imaging

Systems. PLOS ONE 10, e0127121. https://doi.org/10.1371/journal.pone.0127121

Chust, G., Allen, J.I., Bopp, L., Schrum, C., Holt, J., Tsiaras, K., Zavatarelli, M., Chifflet, M., Cannaby, H., Dadou, I., Daewel, U., Wakelin, S.L., Machu, E., Pushpadas, D., Butenschon, M., Artioli, Y., Petihakis, G., Smith, C., Garçon, V., Goubanova, K., Le Vu, B., Fach, B.A., Salihoglu, B., Clementi, E., Irigoien, X., 2014. Biomass changes and trophic amplification of plankton in a warmer ocean. Glob. Change Biol. 20, 2124–2139. https://doi.org/10.1111/gcb.12562

Conway, D.V.P., 2006. Identification of the copepodite developmental stages of twenty-six North Atlantic copepods.

Davies, K.T.A., Vanderlaan, A.S.M., Smedbol, R.K., Taggart, C.T., 2015. Oceanographic connectivity between right whale critical habitats in Canada and its influence on whale abundance indices during 1987–2009. J. Mar. Syst. 150, 80–90. https://doi.org/10.1016/j.jmarsys.2015.05.005

Davis, C., Gallager, S., Berman, M., Haury, L., Strickler, J., 1992. The Video Plankton Recorder (VPR): design and initial results. Arch. Hydrobiol. Beih 36, 67–81.

Deutsch, C., Kuttenkeuler, J., Melin, T., 2020. Glider performance analysis and intermediate-fidelity modelling of underwater vehicles. Ocean Eng. 210, 107567. https://doi.org/10.1016/j.oceaneng.2020.107567

Ellen, J., Hongyu Li, Ohman, M.D., 2015. Quantifying California current plankton samples with efficient machine learning techniques, in: OCEANS 2015 - MTS/IEEE Washington. Presented at the OCEANS 2015 - MTS/IEEE Washington, IEEE, Washington, DC, pp. 1–9. https://doi.org/10.23919/OCEANS.2015.7404607

Ellen, J.S., Graff, C.A., Ohman, M.D., 2019. Improving plankton image classification using context metadata. Limnol. Oceanogr. Methods 17, 439–461. https://doi.org/10.1002/lom3.10324

Folt, C.L., Burns, C.W., 1999. Biological drivers of zooplankton patchiness. Trends Ecol. Evol. 14, 300–305. https://doi.org/10.1016/S0169-5347(99)01616-X

Forest, A., Stemmann, L., Picheral, M., Burdorf, L., Robert, D., Fortier, L., Babin, M., 2012. Size distribution of particles and zooplankton across the shelf-basin system in southeast Beaufort Sea: combined results from an Underwater Vision Profiler and vertical net tows. Biogeosciences 9, 1301–1320. https://doi.org/10.5194/bg-9-1301-2012

Gavrilchuk, K., Lesage, V., Ramp, C., Sears, R., Bérubé, M., Bearhop, S., Beauplet, G., 2014. Trophic niche partitioning among sympatric baleen whale species following the collapse of groundfish stocks in the Northwest Atlantic. Mar. Ecol. Prog. Ser. 497, 285–301. https://doi.org/10.3354/meps10578

Giering, S.L.C., Culverhouse, P.F., Johns, D.G., McQuatters-Gollop, A., Pitois, S.G., 2022. Are plankton nets a thing of the past? An assessment of in situ imaging of zooplankton for large-scale ecosystem assessment and policy decision-making. Front. Mar. Sci. 9, 986206. https://doi.org/10.3389/fmars.2022.986206

Gorsky, G., Ohman, M.D., Picheral, M., Gasparini, S., Stemmann, L., Romagnan, J.-B., Cawood, A., Pesant, S., Garcia-Comas, C., Prejger, F., 2010. Digital zooplankton image analysis using the ZooScan integrated system. J. Plankton Res. 32, 285–303. https://doi.org/10.1093/plankt/fbp124

Grieve, B.D., Hare, J.A., Saba, V.S., 2017. Projecting the effects of climate change on Calanus finmarchicus distribution within the U.S. Northeast Continental Shelf. Sci. Rep. 7, 6264. https://doi.org/10.1038/s41598-017-06524-1

Grosjean, P., Picheral, M., Warembourg, C., Gorsky, G., 2004. Enumeration, measurement, and identification of net zooplankton samples using the ZOOSCAN digital imaging system. ICES J. Mar. Sci. 61, 518–525. https://doi.org/10.1016/j.icesjms.2004.03.012

Guihen, D., Brearley, J.A., Fielding, S., 2022. Antarctic krill likely avoid underwater gliders. Deep Sea Res. Part Oceanogr. Res. Pap. 179, 103680. https://doi.org/10.1016/j.dsr.2021.103680

Harris, R., Weibe, P., Lenz, L., Skjoldal, H., Huntley, M., 2000. ICES zooplankton methodology manual. Elsevier.

Hays, G.C., Proctor, C.A., John, A.W.G., Warner, A.J., 1994. Interspecific differences in the diel vertical migration of marine copepods: The implications of size, color, and morphology. Limnol. Oceanogr. 39, 1621–1629. https://doi.org/10.4319/lo.1994.39.7.1621

Head, E.J.H., Johnson, C.L., Pepin, P., 2022. Plankton monitoring in the Northwest Atlantic: a comparison of zooplankton abundance estimates from vertical net tows and Continuous Plankton Recorder sampling on the Scotian and Newfoundland shelves, 1999–2015. ICES J. Mar. Sci. 79, 901–916. https://doi.org/10.1093/icesjms/fsab208

Helenius, L.K., Head, E.J.H., Jekielek, P., Orphanides, C.D., Pepin, P., Perrin, G., Plourde, S., Ringuette, M., Runge, J.A., Walsh, H.J., Johnson, C.L., 2024. Spatial variability in size and lipid content of the marine copepod *Calanus finmarchicus* across the Northwest Atlantic continental shelves: implications for North Atlantic right whale prey quality. J. Plankton Res. 46, 25–40. https://doi.org/10.1093/plankt/fbad047

Hetherington, E.D., Damian-Serrano, A., Haddock, S.H.D., Dunn, C.W., Choy, C.A., 2022. Integrating siphonophores into marine food-web ecology. Limnol. Oceanogr. Lett. 7, 81–95. https://doi.org/10.1002/lol2.10235

Hoogenboom, J.L., Wong, S.N.P., Ronconi, R.A., Koopman, H.N., Murison, L.D., Westgate, A.J., 2015. Environmental predictors and temporal patterns of basking shark (Cetorhinus maximus) occurrence in the lower Bay of Fundy, Canada. J. Exp. Mar. Biol. Ecol. 465, 24–32. https://doi.org/10.1016/j.jembe.2015.01.005

Horne, J.K., Swan, J.A., Tracy, T.J., Holtgrieve, G.W., 2023. Automated acoustic monitoring of fish for near-real-time resource management. ICES J. Mar. Sci. fsad196. https://doi.org/10.1093/icesjms/fsad196

Irisson, J.-O., Ayata, S.-D., Lindsay, D.J., Karp-Boss, L., Stemmann, L., 2022. Machine Learning for the Study of Plankton and Marine Snow from Images. Annu. Rev. Mar. Sci. 14, 277–301. https://doi.org/10.1146/annurev-marine-041921-013023

Johnson, W.S., Allen, D.M., 2012. Zooplankton of the Atlantic and Gulf coasts: a guide to their identification and ecology., 2nd ed. The John Hopkins University Press.

Johnston, D., Thorne, L., Read, A., 2005. Fin whales Balaenoptera physalus and minke whales Balaenoptera acutorostrata exploit a tidally driven island wake ecosystem in the Bay of Fundy. Mar. Ecol. Prog. Ser. 305, 287–295. https://doi.org/10.3354/meps305287

Lampert, W., 1989. The Adaptive Significance of Diel Vertical Migration of Zooplankton. Funct. Ecol. 3, 21. https://doi.org/10.2307/2389671

Lesage, V., Gosselin, J.-F., Lawson, J.W., McQuinn, I., Moors-Murphy, H., Plourde, S., Sears, R., Simard, Y., 2018. Habitats important to blue whales (Balaenoptera musculus) in the western North Atlantic.

Lewis, M.K., Sameoto, D., 1988. The Vertical Distribution of Zooplankton and lchthyoplankton on the Nova Scotia Shelf October 198.

Lombard, F., Boss, E., Waite, A.M., Vogt, M., Uitz, J., Stemmann, L., Sosik, H.M., Schulz, J., Romagnan, J.-B., Picheral, M., Pearlman, J., Ohman, M.D., Niehoff, B., Möller, K.O., Miloslavich, P., Lara-Lpez, A., Kudela, R., Lopes, R.M., Kiko, R., Karp-Boss, L., Jaffe, J.S., Iversen, M.H., Irisson, J.-O., Fennel, K., Hauss, H., Guidi, L., Gorsky, G., Giering, S.L.C., Gaube, P., Gallager, S., Dubelaar, G., Cowen, R.K., Carlotti, F., Briseño-Avena, C., Berline, L., Benoit-Bird, K., Bax, N., Batten, S., Ayata, S.D., Artigas, L.F., Appeltans, W., 2019. Globally Consistent Quantitative Observations of Planktonic Ecosystems. Front. Mar. Sci. 6, 196. https://doi.org/10.3389/fmars.2019.00196

Maps, F., Storożenko, P.P., Świeżewski, J., Ayata, S.-D., 2024. Automatic estimation of lipid content from *in situ* images of Arctic copepods using machine learning. J. Plankton Res. 46, 41–47. https://doi.org/10.1093/plankt/fbad048

Martin, J.L., Hanke, A.R., LeGresley, M.M., 2009. Long term phytoplankton monitoring, including harmful algal blooms, in the Bay of Fundy, eastern Canada. J. Sea Res. 61, 76–83. https://doi.org/10.1016/j.seares.2008.05.011

Martin-Cabrera, P., Perez, R., Irisson, J.-O., Lombard, F., Möller, K.O., Rühl, S., Creach, V., Lindh, M., Stemmann, L., Schepers, L., 2022. Best practices and recommendations for plankton imaging data management. Version 1.

Meyer-Gutbrod, E., Greene, C., Davies, K., 2018. Marine Species Range Shifts Necessitate Advanced Policy Planning: The Case of the North Atlantic Right Whale. Oceanography 31. https://doi.org/10.5670/oceanog.2018.209

Meyer-Gutbrod, E., Greene, C., Davies, K., Johns, D., 2021. Ocean Regime Shift is Driving Collapse of the North Atlantic Right Whale Population. Oceanography 34, 22–31. https://doi.org/10.5670/oceanog.2021.308

Meyer-Gutbrod, E.L., Davies, K.T.A., Johnson, C.L., Plourde, S., Sorochan, K.A., Kenney, R.D., Ramp, C., Gosselin, J., Lawson, J.W., Greene, C.H., 2022. Redefining North Atlantic right whale habitat-use patterns under climate change. Limnol. Oceanogr. lno.12242. https://doi.org/10.1002/lno.12242

Miller, C., 2000. Oil storage variability in Calanus finmarchicus. ICES J. Mar. Sci. 57, 1786–1799. https://doi.org/10.1006/jmsc.2000.0975

Ohman, M.D., 2019. A sea of tentacles: optically discernible traits resolved from planktonic organisms in situ. ICES J. Mar. Sci. 76, 1959–1972. https://doi.org/10.1093/icesjms/fsz184

Ohman, M.D., Davis, R.E., Sherman, J.T., Grindley, K.R., Whitmore, B.M., Nickels, C.F., Ellen, J.S., 2019. *Zooglider:* An autonomous vehicle for optical and acoustic sensing of zooplankton. Limnol. Oceanogr. Methods 17, 69–86. https://doi.org/10.1002/lom3.10301

Ortner, P.B., Cummings, S.R., Aftring, R.P., Edgerton, H.E., 1979. Silhouette photography of oceanic zooplankton. Nature 277, 50–51. https://doi.org/10.1038/277050a0

Ortner, P.B., Hill, L.C., Edgerton, H.E., 1981. In-situ silhouette photography of Gulf Stream zooplankton. Deep Sea Res. Part Oceanogr. Res. Pap. 28, 1569–1576. https://doi.org/10.1016/0198-0149(81)90098-4

Pershing, A.J., Stamieszkin, K., 2020. The North Atlantic Ecosystem, from Plankton to Whales. Annu. Rev. Mar. Sci. 12, 339–359. https://doi.org/10.1146/annurev-marine-010419-010752

Picheral, M., Catalano, C., Brousseau, D., Claustre, H., Coppola, L., Leymarie, E., Coindat, J., Dias, F., Fevre, S., Guidi, L., Irisson, J.O., Legendre, L., Lombard, F., Mortier, L., Penkerch, C., Rogge, A., Schmechtig, C., Thibault, S., Tixier, T., Waite, A., Stemmann, L., 2022. THE UNDERWATER VISION PROFILER 6: AN IMAGING SENSOR OF PARTICLE SIZE SPECTRA AND PLANKTON, FOR AUTONOMOUS AND CABLED PLATFORMS. Limnol. Oceanogr. Methods 20, 115–129. https://doi.org/10.1002/lom3.10475

Picheral, M., Guidi, L., Stemmann, L., Karl, D.M., Iddaoud, G., Gorsky, G., 2010. The Underwater Vision Profiler 5: An advanced instrument for high spatial resolution studies of particle size spectra and zooplankton. Limnol. Oceanogr. Methods 8, 462–473. https://doi.org/10.4319/lom.2010.8.462

Pollina, T., Larson, A.G., Lombard, F., Li, H., Le Guen, D., Colin, S., De Vargas, C., Prakash, M., 2022. PlanktoScope: Affordable Modular Quantitative Imaging Platform for Citizen Oceanography. Front. Mar. Sci. 9, 949428. https://doi.org/10.3389/fmars.2022.949428

Pomerleau, C., Lesage, V., Winkler, G., Rosenberg, B., Ferguson, S.H., 2014. Contemporary Diet of Bowhead Whales (*Balaena mysticetus*) from the Eastern Canadian Arctic Inferred from Fatty Acid Biomarkers. ARCTIC 67, 84. https://doi.org/10.14430/arctic4366

Prieto, R., Janiger, D., Silva, M.A., Waring, G.T., Gonçalves, J.M., 2012. The forgotten whale: a bibliometric analysis and literature review of the North Atlantic sei whale *Balaenoptera borealis*. Mammal Rev. 42, 235–272. https://doi.org/10.1111/j.1365-2907.2011.00195.x

Record, N., Runge, J., Pendleton, D., Balch, W., Davies, K., Pershing, A., Johnson, C., Stamieszkin, K., Ji, R., Feng, Z., Kraus, S., Kenney, R., Hudak, C., Mayo, C., Chen, C., Salisbury, J., Thompson, C., 2019. Rapid Climate-Driven Circulation Changes Threaten Conservation of Endangered North Atlantic Right Whales. Oceanography 32. https://doi.org/10.5670/oceanog.2019.201

Reiss, C.S., Cossio, A.M., Walsh, J., Cutter, G.R., Watters, G.M., 2021. Glider-Based Estimates of Meso-Zooplankton Biomass Density: A Fisheries Case Study on Antarctic Krill (Euphausia superba) Around the Northern Antarctic Peninsula. Front. Mar. Sci. 8, 604043. https://doi.org/10.3389/fmars.2021.604043

Remsen, A., Hopkins, T.L., Samson, S., 2004. What you see is not what you catch: a comparison of concurrently collected net, Optical Plankton Counter, and Shadowed Image Particle Profiling Evaluation Recorder data from the northeast Gulf of Mexico. Deep Sea Res. Part Oceanogr. Res. Pap. 51, 129–151. https://doi.org/10.1016/j.dsr.2003.09.008

Richardson, A.J., 2008. In hot water: zooplankton and climate change. ICES J. Mar. Sci. 65, 279–295. https://doi.org/10.1093/icesjms/fsn028

Robinson, K.L., Luo, J.Y., Sponaugle, S., Guigand, C., Cowen, R.K., 2017. A Tale of Two Crowds: Public Engagement in Plankton Classification. Front. Mar. Sci. 4. https://doi.org/10.3389/fmars.2017.00082

Ruckdeschel, G.S., Davies, K.T.A., Ross, T., 2020. Biophysical Drivers of Zooplankton Variability on the Scotian Shelf Observed Using Profiling Electric Gliders. Front. Mar. Sci. 7, 627. https://doi.org/10.3389/fmars.2020.00627

Rudnick, D.L., Davis, R.E., Eriksen, C.C., Fratantoni, D.M., Perry, M.J., 2004. Underwater Gliders for Ocean Research. Mar. Technol. Soc. J. 38, 73–84. https://doi.org/10.4031/002533204787522703

Runge, J.A., 1988. Should we expect a relationship between primary production and fisheries? The role of copepod dynamics as a filter of trophic variability. Hydrobiologia 167–168, 61–71. https://doi.org/10.1007/BF00026294

Sahoo, A., Dwivedy, S.K., Robi, P.S., 2019. Advancements in the field of autonomous underwater vehicle. Ocean Eng. 181, 145–160. https://doi.org/10.1016/j.oceaneng.2019.04.011

Schlimpert, O., Uhlmann, D., Schüller, M., Höhne, E., 1980. Automated pattern recognition of phytoplankton–procedure and results. Int. Rev. Gesamten Hydrobiol. Hydrogr. 65, 427–437.

Schminke, H.K., 2007. Entomology for the copepodologist. J. Plankton Res. 29, i149–i162. https://doi.org/10.1093/plankt/fbl073

Schofield, O., Kohut, J., Aragon, D., Creed, L., Graver, J., Haldeman, C., Kerfoot, J., Roarty, H., Jones, C., Webb, D., Glenn, S., 2007. Slocum Gliders: Robust and ready. J. Field Robot. 24, 473–485. https://doi.org/10.1002/rob.20200

Schröder, S.-M., Kiko, R., Koch, R., 2020. MorphoCluster: Efficient Annotation of Plankton images by Clustering.

Sieracki, C., Sieracki, M., Yentsch, C., 1998a. An imaging-in-flow system for automated analysis of marine microplankton. Mar. Ecol. Prog. Ser. 168, 285–296. https://doi.org/10.3354/meps168285

Sieracki, C., Sieracki, M., Yentsch, C., 1998b. An imaging-in-flow system for automated analysis of marine microplankton. Mar. Ecol. Prog. Ser. 168, 285–296. https://doi.org/10.3354/meps168285

Simon, M., Grossart, H., Schweitzer, B., Ploug, H., 2002. Microbial ecology of organic aggregates in aquatic ecosystems. Aquat. Microb. Ecol. 28, 175–211. https://doi.org/10.3354/ame028175

Sims, D., Merrett, D., 1997. Determination of zooplankton characteristics in the presence of surface feeding basking sharks Cetorhinus maximus. Mar. Ecol. Prog. Ser. 158, 297–302. https://doi.org/10.3354/meps158297

Sorochan, K.A., Plourde, S., Johnson, C.L., 2023. Near-bottom aggregations of *Calanus* spp. copepods in the southern Gulf of St. Lawrence in summer: significance for North Atlantic right whale foraging. ICES J. Mar. Sci. 80, 787–802. https://doi.org/10.1093/icesjms/fsad003

Tarrant, A., Baumgartner, M., Verslycke, T., Johnson, C., 2008. Differential gene expression in diapausing and active Calanus finmarchicus (Copepoda). Mar. Ecol. Prog. Ser. 355, 193–207. https://doi.org/10.3354/meps07207

Tarrant, A.M., Baumgartner, M.F., Hansen, B.H., Altin, D., Nordtug, T., Olsen, A.J., 2014. Transcriptional profiling of reproductive development, lipid storage and

molting throughout the last juvenile stage of the marine copepod Calanus finmarchicus. Front. Zool. 11, 91. https://doi.org/10.1186/s12983-014-0091-8

Trudnowska, E., Lacour, L., Ardyna, M., Rogge, A., Irisson, J.O., Waite, A.M., Babin, M., Stemmann, L., 2021. Marine snow morphology illuminates the evolution of phytoplankton blooms and determines their subsequent vertical export. Nat. Commun. 12, 2816. https://doi.org/10.1038/s41467-021-22994-4

Turner, J.T., Dagg, M.J., 1983. Vertical Distributions of Continental Shelf Zooplankton in Stratified and Isothermal Waters.

Van Guelpen, L., Markle, D.F., Duggan, D.J., 1982. An evaluation of accuracy, precision, and speed of several zooplankton subsampling techniques. ICES J. Mar. Sci. 40, 226–236. https://doi.org/10.1093/icesjms/40.3.226

Whitmore, B.M., Nickels, C.F., Ohman, M.D., 2019a. A comparison between Zooglider and shipboard net and acoustic mesozooplankton sensing systems. J. Plankton Res. 41, 521–533. https://doi.org/10.1093/plankt/fbz033

Whitmore, B.M., Nickels, C.F., Ohman, M.D., 2019b. A comparison between Zooglider and shipboard net and acoustic mesozooplankton sensing systems. J. Plankton Res. 41, 521–533. https://doi.org/10.1093/plankt/fbz033

Wiebe, P.H., Benfield, M.C., 2003. From the Hensen net toward four-dimensional biological oceanography. Prog. Oceanogr. 56, 7–136. https://doi.org/10.1016/S0079-6611(02)00140-4

Wilson, R.J., Banas, N.S., Heath, M.R., Speirs, D.C., 2016. Projected impacts of 21st century climate change on diapause in *Calanus finmarchicus*. Glob. Change Biol. 22, 3332–3340. https://doi.org/10.1111/gcb.13282

Woodley, T.H., Gaskin, D.E., 1996. Environmental characteristics of North Atlantic right and fin whale habitat in the lower Bay of Fundy, Canada. Can. J. Zool. 74, 75–84. https://doi.org/10.1139/z96-010

APPENDIX A. NET SAMPLE PROCESSING PROTOCOL ADAPTED FROM THE ATLANTIC REFERENCE CENTRE

Notes:

- All specimens fixed in 4% buffered formaldehyde (10% formalin).
- After split fractions have been counted they will be preserved in 70% ethanol.

Procedure:

1) Wear lab coat and goggles and nitrile gloves.
2) In the fume hood, decant the sample through a sieve and over a beaker. Save decanted formalin for later use. Make sure to cover decanted formalin.
3) Put on respirator.
4) Transport sample to the sink to rinse well with freshwater.
5) Remove macrozooplankton (>10 mm) from sample and rinse in a beaker of freshwater. Repeat this process twice, making sure to add rinse water back into the sieve with the rest of the sample each time.
6) Save the macrozooplankton separately from the rest of the sample as a 1/1 "split".
7) Transfer sample from sieve to beaker with freshwater.
8) Splitting will be done according to the Huntsman Marine Laboratory beaker technique[1].
9) Once a split with 200 – 300 animals is obtained, species will be sorted and identified to the lowest taxonomic level possible. Of these 200-300 animals, 75 – 100 individuals must be *Calanus.*
10) If there is not 75-100 *Calanus*. after sorting through the original split, sort through another split, pulling only *Calanus.* This means that your *Calanus.* will have a different split than the rest of your animals so be sure to record this.
11) Wet weight measurements:
    a. After identification of the entire sample, blot dry all macrozooplankton and weigh using a digital balance to a precision of 10^{-4}. Repeat this process for mesozooplankton. Record these values separately in the datasheet.
12) Saved all identified individuals in a 4 dram vial with 70% ethanol.
13) Return unsorted portion of sample to original sampling jar and pour the saved formalin back in.

We require from each cruise (n = 1 cruise in BoF in 2020) length and width frequency data from the most common groups.

14) Measure length and width under microscope
15) Choose one net
16) Start with 50 individuals of a particular taxon from any given net. Plot the histogram. If it looks statistically normal with no gaps, then stop. If not, do another 20 etc. up to 100.

17) Measurements: Length and width of all dominant mesozooplankton, likely all microzooplankton-sized euphausiids, *Calanus finmarchicus C3*, *C4*, *C5*, and *C6*, and any species with a gas bladder.

References:

1. Van Guelpen L, Markle DF, Duggan DJ. 1982. An evaluation of accuracy, precision, and speed of several zooplankton subsampling techniques. J. Cons. int. Explor. Mer. 40: 226-236.

APPENDIX B. TAXONOMIC CATEGORIES FROM UVP6

Table 3. Taxonomic categories assigned to UVP6 Regions of Interest. Indented taxa in the left column represent lower taxonomic level (e.g., *Tomopteris* sp. is a genus within the Annelida). Note that species level identification was not typically possible using UVP6 images.

Identification	Description
Actinopterygii	Adults and juveniles
Amphipoda	Adults and juveniles
Annelida	Adults and larvae
Tomopteris sp.	Annelid genus
Appendicularia	Adults and mucus houses
Brachyura	Larvae
Bryozoa	Larvae
Chaetognatha	
Cirripedia	Larvae
Cnidaria	General cnidarians
Hydrozoa	General hydrozoans
Siphonophorae	
Copepoda	General copepods
Calanus sp.	Copepod genus
Paraeuchaeta sp.	Copepod genus
Crustacea	General crustaceans

Ctenophora	
Echinodermata	Larvae
Eumalacostraca	General eumalacostracids
Euphausiacea	
Ostracoda	
Salpidae	Colonial and solitary
detritus	Marine snow
unknown<zooplankton	ROIs that are possibly zooplankton but cannot be confirmed

APPENDIX C. TAXONOMIC CATEGORIES FROM SHADOWGRAPH

Table 4. Taxonomic categories assigned to shadowgraph Regions of Interest. Indented taxa in the left column represent lower taxonomic level (e.g., *Tomopteris* sp. is a genus within Polychaeta).

Identification	Description
Amphipoda	Adults and juveniles
Polychaeta	Adults and larvae
Tomopteris sp.	Polychaete genus
Appendicularia	Adults
Brachyura	Larvae
Chaetognatha	
Cirripedia	Larvae
Hydrozoa	General hydrozoans
Siphonophorae	Adults and larvae
Copepoda	General copepods
Calanus sp.	Copepod genus
Paraeuchaeta sp.	Copepod genus
Centropages sp.	Copepod genus
Oithona sp.	Copepod genus
Crustacea	General crustaceans, adult and nauplius
Ctenophora	
Beroe spp.	Ctenophore genus

Pleurobranchia pileus	Ctenophore species
Echinodermata	Larvae
Euphausiacea	General eumalacostracids, juveniles
Ostracoda	Adults
Salpidae	Colonial and solitary
Marine snow	
Unknown	ROIs that are possibly zooplankton but cannot be confirmed

APPENDIX D. TWO-WAY ANOVA TABLES

Table 9. Two-way ANOVA results for the main effects and interaction of net number (i.e. depth) and day/night on copepod concentrations measured by the MultiNet.

	Sum of Squares	Degrees of Freedom	F value	P value
(Intercept)	40.0074883	1	2143.11084	1.0065E-42
Net	4.02890904	4	53.9548907	1.5414E-17
Day/Night	0.00126798	1	0.06792297	0.79545568
Net:Day/Night	0.07126624	4	0.95439292	0.44071504
Residuals	0.93339755	50		

Table 10. Two-way ANOVA results for the main effects and interaction of net number (i.e. depth) and day/night on copepod concentrations measured by the UVP6.

	Sum of Squares	Degrees of Freedom	F value	P value
(Intercept)	11.2247209	1	89.1249505	1.0753E-12
Net	1.7954112	4	3.56391789	0.01237286
Day/Night	0.04788122	1	0.3801797	0.54030449
Net:Day/Night	0.16203453	4	0.32164094	0.86215673
Residuals	6.29718213	50		

Table 11. Two-way ANOVA results for the main effects and interaction of net number (i.e. depth) and day/night on copepod concentrations measured by the shadowgraph.

	Sum of Squares	Degrees of Freedom	F value	P value
(Intercept)	19.8208935	1	403.079056	5.3726E-25
Net	3.42835427	4	17.4298122	6.7872E-09
Day/Night	0.00389045	1	0.07911655	0.77970723
Net:Day/Night	0.20230637	4	1.02852909	0.40221561
Residuals	2.36033819	48		

Table 12. Two-way ANOVA results for the main effects and interaction of net number (i.e. depth) and day/night on *Calanus* concentrations measured by the MultiNet.

	Sum of Squares	Degrees of Freedom	F value	P value
(Intercept)	29.0979493	1	1600.81995	1.2259E-39
Net	2.69706461	4	37.0946658	2.1445E-14
Day/Night	0.0053952	1	0.29681621	0.58830718
Net:Day/Night	0.04828666	4	0.66412111	0.61986764
Residuals	0.90884516	50		

CURRICULUM VITAE

Candidate's Full Name: Natasha Jessica Hynes

Universities Attended:

2014-2018 Dalhousie University
Bachelor of Science
Major Marine Biology
Minor French

2022-present University of New Brunswick Saint John
Master of Science
Biology

Publications:

Lonati G, **Hynes N**, Howe K, Durette-Morin D, Brown M, Davies K. 2022. Observations of Adult-Calf Nonreproductive Copulatory Behavior in North Atlantic Right Whales (*Eubalaena glacialis*). *Aquatic Mammals*. 48(6), 639-645.

Presentations:

2022 International Conference on Copepoda, World Association of Copepodoloists Oral presentation: "Using a glider-mounted shadowgraph camera to characterize the zooplankton community in the Bay of Fundy, Canada"

2023 6th Workshop on Trait-Based Approaches to Ocean Life, Technical University of Denmark Poster presentation: "A trait-based approach to classifying zooplankton shadowgraph camera images from a profiling autonomous platform in the Bay of Fundy, Canada"

2023 Fundy Whale Fest, Huntsman Marine Science Centre Oral presentation: "Whale Food & Tools We Use to Study It."

2023 North Atlantic Right Whale Consortium Annual Meeting Oral presentation: "A glider-mounted shadowgraph camera for measuring pelagic copepod abdundance and distribution in North Atlantic right whale habitat."

2024 7th International Zooplankton Production Symposium Oral presentation:
"Performance of a plankton imaging system mounted on a profiling glider for censusing zooplankton in threatened predator habitat."